A Discrete Basis Set Technique for Calculating Photoionization Cross Sections Utilizing Moment Theory

Alexander S. Gerwer

Submitted in partial fulfillment of
the requirements for the degree
Master of Science in Chemistry

~~1978~~ 1980

California Institute of Technology
Pasadena, California

Contents

(I) INTRODUCTION

Techniques for measuring the photoionization cross sections of diatomic molecules have improved significantly in the past twenty years.[1,2] Precise ab initio photoionization calculations in the semiclassical approximation, however, have been limited to the simplest of diatomic systems.[3] This is primarily due to difficulties that arise in the construction of many-electron continuum functions appropriate for the unbound motion of an ejected electron in the presence of a nonspherical ionic molecular core. Consequently, ad hoc computational approximations, including the additive atomic approximation,[4] one-center many-body calculations,[5] the use of plane-wave final states,[6] the scattered X_α method,[7] and the use of one- and two-center Coulomb wavefunctions,[8] have been employed in semiclassical photoionization calculations. These techniques require lengthy calculations, are of unknown accuracy and are difficult to systematically improve.

Because computation of many-electron continuum eigenfunctions for diatomic molecules is so difficult, various procedures have been suggested recently for constructing photoionization profiles utilizing the discrete oscillator strengths and transition frequencies which are obtained from variational calculations in Hilbert space.[9-11] These techniques have long been useful in conventional bound-

state configuration-interaction calculations.[12] In particular, the Stieltjes-Tchebyscheff technique,[10,11] based on the theory of moments,[13] can accomodate different types of basis functions and can provide highly reliable photoabsorption cross sections. Stieltjes-Tchebyscheff profiles have been reported for the negative hydrogen,[11b] lithium, sodium, and potassium ions,[14] atomic helium,[10c,11b] lithium,[15] boron,[16] molecular hydrogen,[17] formaldehyde,[18] molecular nitrogen,[19] and carbon monoxide.[20]

In the present report, the Stieltjes-Tchebyscheff technique is employed in calculations of total photoionization cross sections. This procedure can be outlined as follows: Moment theory is used in computing the cummulative oscillator strength distribution of the molecule in question. This is done by employing the static-exchange approximation for the Hartree-Fock ionic core. Various sets of virtual orbitals are created for the electron which is photoejected into the molecular continuum. It is assumed that the various physically distinct excitations, or channels, of the molecule are independent of each other. This approximation greatly simplifies the computations and avoids possible spurious results caused by weak channel interactions. Each channel is separated into its individual components as defined by the various allowed final states in which the molecule could be left by excitation. An appropriate set of virtual

orbitals is generated using a basis set of normalizable Gaussian functions. The oscillator strength distribution can be computed from the dipole-allowed transitions between the ground state and the virtual orbitals.[19] The energies of the virtuals and the corresponding oscillator strengths serve as points and weights, respectively, of a histogram approximation to the true cross section. The total cross section is taken as the sum of each individual spectrum computed in this manner.

In the case of O_2 we looked at the three main ionizations that contribute to the total cross section; $^3\Sigma_g^- + h\nu \rightarrow X^2\Pi_g + e^-$, $^3\Sigma_g^- + h\nu \rightarrow (a^2\Pi_u + A^4\Pi_u) + e^-$, and $^3\Sigma_g^- + h\nu \rightarrow (b^2\Sigma_g^- + B^4\Sigma_g^-) + e^-$ in the case of valence shell photoionization. There are eight possible allowed final states connecting these ionizations to the O_2 ground state. A partial cross section was computed for each channel by taking the sum of the components which describe that channel. These partial cross sections showed considerable agreement with the available experimental data. The sum of these three channels yielded the total cross section, in good agreement with experiments.

We were also able to show that the Stieltjes method provided reliable results for inner shell photoionization cross sections. We computed the cross section for ionization out of the K-shell in the oxygen molecule. Again, the results obtained were consistent with experimental data.

In summary, the separated-channel, static-exchange calculations employing the Stieltjes-Tchebyscheff procedure yielded excellent first approximations to photoionization processes in molecular oxygen, a complex, open shell system. It should be possible to obtain cross sections for a variety of complex molecules using this technique, and hence avoid the involved and lengthy computations that have previously been required to construct the spectra of complex molecules. Future work could also involve calculation of angular distributions of photoejected electrons using integrated partial cross sections in conjunction with the scattering theory of asymptotic phases of the continuum orbital wavefunction.

The Stieltjes-Tchebyscheff technique is detailed in Section II. Section III provides a look at the direction in which future work will procede. The Appendix consists of two papers (in preprint form) in which we have applied the Stieltjes-Tchebyscheff technique to molecular oxygen.

(II) THEORY

This section starts with the concept of a complex dynamic dipole polarizability and procedes to develope the Stieltjes imaging technique. In the last subsection, a simple case is worked out as an example.

A) The Complex Polarizability

The interaction of radiation with matter is described by the time-dependent Schrödinger equation[21]

$$[H^{(0)}(\underline{r}) + H^{(1)}(\underline{r},t) - i(\partial/\partial t)]\psi(\underline{r},t) = 0, \tag{1}$$

where $H^{(0)}(\underline{r})$ is the field-free Hamiltonian and, in the semiclassical approximation,[22]

$$H^{(1)}(\underline{r},t) = \mu(\underline{r})\cos\omega t \tag{2a}$$

with

$$\mu(\underline{r}) = -\sum_{i=1}^{N} \underline{a}\cdot\underline{r}_i, \tag{2b}$$

being the component of the electric dipole moment operator for an N-electron system in the direction of polarization of the (unit) electric intensity $\underline{a}$. The latter is chosen along a principal axis of the polarizability tensor for simplicity. The symbol $\underline{r}$ represents all appropriate spin and space coordinates.

The wavefunction $\psi(\underline{r},t)$ can be expanded in a perturbation series up to first order

$$\psi(\underline{r},t) = \psi^{(0)}(\underline{r},t) + \psi^{(1)}(\underline{r},t) + \ldots, \tag{3}$$

where $$\psi^{(0)}(\underline{r},t) = \phi^{(0)}(\underline{r})\exp(-iE^{(0)}t) \tag{4}$$

$$\psi^{(1)}(\underline{r},t) = [\phi_+^{(1)}(\underline{r})\exp(i\omega t) + \phi_-^{(1)}(\underline{r})\exp(-i\omega t)] \times \tfrac{1}{2}\exp(-iE^{(0)}t) \tag{5}$$

where the function $\phi^{(0)}(\underline{r})$ is an eigenstate of the unperturbed Hamiltonian and $\phi_{\pm}^{(1)}$ is the particular solution of

$$[H^{(0)}(\underline{r}) - E^{(0)} \pm \omega]\phi_{\pm}^{(1)}(\underline{r}) + \mu(\underline{r})\phi^{(0)}(\underline{r}) = 0 \tag{6}$$

that is orthogonal to $\phi^{(0)}(\underline{r})$. Expanding the solution of eqn. (6) in terms of the complete set of discrete and continuum eigenfunctions $[\phi_i^{(0)}(\underline{r}), \phi_E^{(0)}(\underline{r})]$ of $H^{(0)}(\underline{r})$,

$$\phi_{\pm}^{(1)}(\underline{r}) = -\sum_{i=1}^{\infty} \frac{\langle\phi_i^{(0)}|\mu|\phi^{(0)}\rangle}{\varepsilon_i \pm \omega}\phi_i^{(0)}(\underline{r}) - \int_0^{\infty} \frac{\langle\phi_E^{(0)}|\mu|\phi^{(0)}\rangle}{\varepsilon \pm \omega}\phi_E^{(0)}(\underline{r})dE, \tag{7}$$

where $\varepsilon_i = E_i^{(0)} - E^{(1)}$ are the discrete and $\varepsilon = E - E^{(0)}$ the continuum transition frequencies, with the continuum eigenfunctions $\phi_E^{(0)}(\underline{r})$ delta-function normalized in energy.[23]

The induced electric dipole moment along the direction of the unit electric field intensity $\underline{a}$ is

$$D(\omega,t) = \langle\psi^{(0)}|\mu|\psi^{(1)}\rangle + \langle\psi^{(1)}|\mu|\psi^{(0)}\rangle \ .$$

Substituting for $\psi^{(0)}$ and $\psi^{(1)}$ from eqns. (4) and (5), respectively,

$$D(\omega,t) = \alpha(\omega)\cos\omega t, \tag{8}$$

where the frequency-dependent dipole polarizability is given by

$$\alpha(\omega) = \langle\phi^{(0)}|\mu|\phi_+^{(1)}\rangle + \langle\phi_-^{(1)}|\mu|\phi^{(0)}\rangle \ .$$

If we use the expression for $\phi_{\pm}^{(1)}(\underline{r})$ given in eqn. (7) along with the orthonormality of the set $[\phi_i^{(0)}(\underline{r}), \phi_E^{(0)}(\underline{r})]$, we may write

$$\alpha(\omega) = \sum_{i=1}^{\infty} \frac{f_i}{\varepsilon_i^2 - \omega^2} + \int_{\omega_t}^{\infty} \frac{g(\varepsilon)}{\varepsilon^2 - \omega^2}\, d\varepsilon, \tag{9}$$

with ω_t the photoionization threshold frequency and

$$f_i = 2\varepsilon_i |\langle \phi_i^{(0)} | \mu | \phi^{(0)} \rangle|^2 \tag{10a}$$

$$g(\varepsilon) = 2\varepsilon \, |\langle \phi_E^{(0)} | \mu | \phi^{(0)} \rangle|^2 \tag{10b}$$

the oscillator strengths and density for discrete and continuum transitions, respectively. Equation (9) can be formulated as a Riemann-Stieltjes integral,

$$\alpha(z) = \int_{\varepsilon_1}^{\infty} \frac{df(\varepsilon)}{(\varepsilon^2 - z^2)} , \tag{11}$$

where the result has been continued to the entire complex frequency plane, ε_1 is the resonance frequency, and

$$\int_0^{\varepsilon} df(\varepsilon') = \int_0^{\varepsilon} \left[\sum_{i=1}^{\infty} f_i \, \delta(\varepsilon_i - \varepsilon') + g(\varepsilon') \right] d\varepsilon'$$

$$= f(\varepsilon) \tag{12}$$

is the cummulative oscillator strength. The dynamic complex polarizability is analytic throughout the complex z-plane except for an infinite number of simple poles on the real axis at $z = \pm\varepsilon_i$ and a branch cut along the real axis in the photoionization interval $\omega_t \leq |\omega| < \infty$. The behavior of $\alpha(z)$ across the real axis in the photo-

ionization interval can be shown from its behavior in the neighborhood of $z = \omega \pm i\delta$ as $\delta \to o$.

$$\alpha(\omega \pm io) = Re\alpha(\omega) \pm iIm\alpha(\omega), \tag{13}$$

where $$Re\alpha(\omega) = P \int_{\varepsilon_i}^{\infty} \frac{df(\varepsilon)}{\varepsilon^2 - \omega^2} \tag{14b}$$

and $$Im\alpha(\omega) = \pi g(\omega)/2\omega, \tag{14b}$$

with P implying the Cauchy principal value.[24] Both the photoabsorption and dispersion profiles are contained in $\alpha(z)$, since, under appropriate conditions, the photoabsorption cross section is[25]

$$\sigma(\omega) = \frac{2\pi^2}{c} g(\omega)$$

$$\sigma(\omega) = \frac{4\pi\omega}{c} Im\alpha(\omega) \tag{15a}$$

and the refractive index is given by[26]

$$n(\omega) - 1 = 2\pi N_o Re\alpha(\omega) \tag{15b}$$

with c the speed of light and N_o the number of molecules.

B) Quadrature Approximation to the Spectral Resolution

The completeness of the set of electronic eigenfunctions of the Born-Oppenheimer Hamiltonian, H, allows an eigenfunction expansion or spectral resolution for H

$$H = \sum_i |\phi_i\rangle E_i \langle\phi_i| + \int_o^\infty dE\, |\phi(E)\rangle E \langle\phi(E)|, \tag{16}$$

where the $|\phi_i\rangle$ are bound state square-integrable eigenfunctions

$$H|\phi_i\rangle = E_i|\phi_i\rangle, \tag{17}$$

with the orthonormality condition

$$\langle\phi_i|\phi_j\rangle = \delta_{ij}, \tag{18}$$

and the $|\phi(E)\rangle$ are continuum eigenfunctions

$$H|\phi(E)\rangle = E|\phi(E)\rangle, \tag{19}$$

which are delta-function normalized

$$\langle\phi(E)|\phi(E')\rangle = \delta(E-E') \ . \tag{20}$$

Only a subspace defined by a single non-degenerate symmetry is considered in eqn. (16).[27] Thus, for each symmetry,

the complete set of eigenfunctions may be expressed as a sum over bound states and an integral over the continuum whose origin has been chosen at E = 0.

In an improved virtual orbital calculation,[28] a finite basis of square-integrable functions (e.g. Slater determinants composed of molecular orbitals, which are in turn expanded in terms of Gaussian orbitals) is employed. The matrix representation of the Hamiltonian, $\hat{H}$, is diagonalized to give a set of approximate eigenfunctions, $|\chi_i>$, and eigenvalues $\tilde{E}_i$,

$$\tilde{H}|\chi_i> = \tilde{E}_i|\chi_i>, \tag{21}$$

appropriately normalized

$$<\chi_i|\chi_j> = \delta_{ij}. \tag{22}$$

Within the subspace defined by the choice of basis, the spectral resolution of $\tilde{H}$ can be expressed as

$$\tilde{H} = \sum_{E_i<0} |\chi_i> \tilde{E}_i <\chi_i| + \sum_{E_j>0} |\chi_j> \tilde{E}_j <\chi_j|. \tag{23}$$

Here the sum over approximate eigenfunctions has been divided into a portion over negative eigenvalues which

intuitively corresponds to the bound state sum of eqn. (16), and a portion over positive eigenvalues which is expected to approximate the continuum. It has been shown[29] that

$$\sum_{E_j>0} |\chi_j>\tilde{E}_j<\chi_j| \approx \int_0^\infty dE|\phi(E)>E<\phi(E)| \tag{24}$$

when properly interpreted as a numerical quadrature. Specifically, to evaluate a matrix element such as

$$<\psi|H|\psi> = \sum_i <\psi|\phi_i>E_i<\phi_i|\psi> + \int_0^\infty dE<\psi|\phi(E)>E<\phi(E)|\psi>, \tag{25}$$

where $|\psi>$ is an arbitrary square-integrable function, one might, in a purely numerical sense, evaluate the continuum part of the matrix element as

$$\int_0^\infty dE<\psi|\phi(E)>E<\phi(E)|\psi> \approx \sum_j \omega_j <\psi|\phi(E_j)>E_j<\phi(E_j)|\psi>, \tag{26}$$

where the E_j and ω_j are appropriate numerical quadrature abscissas and weights, respectively. This is just the standard numerical technique of replacing an integral by a quadrature sum.[30] Following the suggestion of eqn. (24), the quadrature approximation of eqn. (16) should be related to the approximation of the continuum part of $<\psi|H|\psi>$ as

$$\int_0^\infty dE<\psi|\phi(E)>E<\phi(E)|\psi> \approx \sum_{E_j>0} <\psi|\chi_j>E_j<\chi_j|\psi>. \tag{27}$$

In both eqns. (24) and (26) an integral is to be replaced by a sum. In eqn. (26) the sum is generated by choosing a specific numerical quadrature, while in eqn. (24) the sum arises directly from the diagonalization of $\tilde{H}$. In certain cases[29,31] the seemingly distinct approximations of eqns. (24) and (26) not only yield equivalent results for $\langle\psi|H|\psi\rangle$ but the sums are identical term by term. Thus, the square-integrable functions, $|\chi_j\rangle$ $[\tilde{E}_j>0]$, are proportional to the continuum functions, $\phi(\tilde{E}_j)$, evaluated at the same energy. When this is the case, photoionization information (at energy E_j) may be easily extracted directly from the $|\chi_j\rangle$.

Interpreted more generally, the square-integrable eigenfunctions arising from discretization of an arbitrary electronic Hamiltonian in an arbitrary square-integrable basis give a quadrature representation of the actual spectrum of eigenvalues and eigenfunctions of the Hamiltonian itself. This implicit quadrature is refered to as the equivalent quadrature[29] generated by the Hamiltonian and the basis.

C) Photoionization: Equivalent Quadrature Unknown

Equation (23) is interpreted as a quadrature representation. Thus

$$|\chi_i\rangle = (\omega_i{}^{Eq})^{\frac{1}{2}}|\phi(\tilde{E}_i)\rangle \quad [\tilde{E}_i>0], \tag{28}$$

where $\phi(\tilde{E}_i)$ is the actual electronic continuum state at energy $\tilde{E}_i$ and ω_i^{Eq} is the equivalent quadrature weight implicit in the choice of basis. Equation (28) holds over a limited range of coordinate space. When this range spans the range of $\underset{\sim}{\mu}|\Phi\rangle$ where Φ is the N-electron ground state wave function, the transition amplitude can be computed

$$\langle\phi(\tilde{E}_i)|\underset{\sim}{\mu}|\Phi\rangle \approx (\omega_i^{Eq})^{-\frac{1}{2}}\langle\chi_i|\underset{\sim}{\mu}|\Phi\rangle \qquad (29)$$

provided that the equivalent quadrature weights are independently known. For an arbitrary N-electron system, however, the equivalent quadrature implicit in the basis discretization will not be known. Thus photoionization information cannot be extracted directly from the states $|\chi_i\rangle$.

Nevertheless, because a quadrature is implicit in the discretized spectral resolution, matrix elements of the form

$$\sigma^k = \langle\Phi|\underset{\sim}{\mu}H^k\underset{\sim}{\mu}|\Phi\rangle =$$

$$\langle\Phi|\underset{\sim}{\mu}\left\{\sum_i|\phi_i\rangle E_i^k\langle\phi_i| + \int_o^\infty dE|\phi(E)\rangle E^k\langle\phi(E)|\right\}\underset{\sim}{\mu}|\Phi\rangle$$

$$\approx \langle\Phi|\underset{\sim}{\mu}\sum_j|\chi_j\rangle\tilde{E}_j^k\langle\chi_j|\underset{\sim}{\mu}|\Phi\rangle \qquad k = 1,2,3,... \qquad (30)$$

which involve summation and integration over the whole spectrum of the operator can be approximated. Regrouping terms in eqn. (30)

$$\langle\Phi|\underset{\sim}{\mu}H^k\underset{\sim}{\mu}|\Phi\rangle = \sum_i \sigma_i E_i^k + \int_o^\infty \sigma(E)E^k dE, \tag{31}$$

where $$\sigma(E) = |\langle\Phi|\underset{\sim}{\mu}|\phi(E)\rangle|^2 \tag{32a}$$

and $$\sigma_i = |\langle\Phi|\underset{\sim}{\mu}|\phi_i\rangle|^2 \tag{32b}$$

are proportional to the photoionization cross section and bound-bound oscillator strengths, respectively. Thus $\langle\Phi|\underset{\sim}{\mu}H^k\underset{\sim}{\mu}|\Phi\rangle$ gives the k^{th} moment of the photoabsorption cross section which, according to eqn. (30) is approximated, in a quadrature sense, by

$$\sigma^k \approx \sum_i \tilde{\sigma}_i \tilde{E}_i^k \tag{33}$$

where $$\tilde{\sigma}_i = |\langle\Phi|\underset{\sim}{\mu}|\chi_i\rangle|^2 \tag{34}$$

Thus, although for an arbitrary basis $\sigma(E)$ cannot be calculated directly at the energies $\tilde{E}_i$ because of a lack of knowledge of the equivalent quadrature weights, the moments of the cross section can be calculated. Each of the moments σ^k represents a smoothing of the distribution

of transition moments $\tilde{\sigma}_i$ calculated in the square-integrable basis set. When the basis is enlarged, the converged low order moments represent the useful information contained in the improved virtual orbital calculation.

D) Extraction of $\sigma(E)$ from its Moments

The method for constructing $\sigma(E)$ from its moments σ^k can be developed from the theory of Gaussian integration.[30] To approximate

$$\int_a^b \rho(x)h(x)dx \ , \tag{35}$$

a sum of the form

$$\sum_{i=1}^{n} h(x_i)\omega_i \tag{36}$$

is constructed. $\rho(x)$ is a known weight function and $h(x)$ is the well-behaved function to be integrated. First, the monomials x^n, $n = 0,1,2,\ldots$ are integrated; that is, the moments

$$M(k) = \int_a^b \rho(x)x^k dx \tag{37}$$

are determined. When quadrature approximations are used for the moments, eqn. (37) leads to

$$M(o) = \int_a^b \rho(x)dx = \sum_{i=1}^{n} \omega_i {}^{\rho}x_i{}^{o} \tag{38a}$$

$$M(1) = \int_a^b \rho(x)xdx = \sum_{i=1}^{n} \omega_i {}^{\rho}x_i{}^{1} \tag{38b}$$

$$\vdots$$

$$M(2n-1) = \int_a^b \rho(x)x^{2n-1}dx = \sum_{i=1}^{n} \omega_i {}^{\rho}x_i{}^{2n-1} . \tag{38c}$$

The solution of this set of 2n non-linear equations for the 2n unknowns $\{\omega_i{}^{\rho}, x_i\}$ yields a set of quadrature weights and abscissas such that the approximation

$$\int_a^b \rho(x)h(x)dx = \sum_{i=1}^{n} \omega_i {}^{\rho}h(x_i) \tag{39}$$

is exact if h(x) is a polynomial of degree 2n-1 or less. Thus, given the moments σ^k, a quadrature can be constructed to evaluate

$$\int_a^b \sigma(E)h(E)dE$$

for arbitrary h(E). An approximation to σ(E) itself, however, is needed. Here the idea of a Stieltjes approximation and Stieltjes imaging[10] enters. Stieltjes[32] suggested that if

$$\int_a^b \rho(x)dx = \sum_{i=1}^{n} \omega_i {}^{\rho}, \tag{40a}$$

then
$$\int_a^y \rho(x)dx \simeq \sum_{i=1}^{n^*} \omega_i \rho, \tag{40b}$$

where $a \leq y < b$ and the integer n^* is chosen such that $x_{n^*} < y < x_{n^*+1}$. This gives a histogram representation of the integral, with the rigorous Tchebyscheff bounding property.[32]

$$\sum_{i=1}^{n^*} \omega_i \rho \leq \int_a^{x_{n^*}} \rho(x)dx \leq \sum_{i=1}^{n^*+1} \omega_i \rho. \tag{41}$$

More importantly the midpoint of each "rise", i.e.

$$\tfrac{1}{2}\left| \sum_{i=1}^{n^*} \omega_i \rho + \sum_{i=1}^{n^*+1} \omega_i \rho \right|,$$

gives a remarkable approximation to the integral at the points of increase, x_{n^*} This being the case, these midpoints can be interpolated with a "smooth" analytic fit which can be differentiated.

$$\frac{d}{dy}\int_a^y \rho(x)dx = \rho(y) \tag{42}$$

to give the weight function, ρ, itself.

For photoionization the quadrature weights and abscissas (ω_i^{σ}, E_i) can be obtained from the moments σ^k by solving a set of moment equations analogous to those of eqns. (38). Thus, the Stieltjes approximation to

$$\int_0^E \sigma(E')dE' \tag{43}$$

can be found and finally differentiated to form $\sigma(E)$ itself. Note that the weights ω_i^{σ} derived via this process are the quadrature weights generated by the positive definite distribution $\sigma(E)$, rather than the equivalent quadrature weights ω_i^{Eq} discussed in Section IIC, which are generated directly by diagonalization of $\tilde{H}$.

In practice, rather than calculating approximate moments of the photoabsorption cross section, it is convenient to work with the oscillator strength distribution of eqn. (12) of Section IIA. According to eqn. (15a), the oscillator strength at each energy differs from the absorption cross section by a known factor. Thus Stieltjes imaging of the negative moments

$$S(-k) = \int_{\varepsilon_i}^{\infty} \varepsilon^{-k} df(\varepsilon) \tag{44}$$

of the oscillator strength distribution will immediately allow construction of the photoionization cross section.

In approximate calculations the moments are calculated as

$$\tilde{S}(-k) = \sum_{i=1}^{n} \tilde{\varepsilon}_i^{-k} \tilde{f}_i \ , \tag{45}$$

where $\tilde{\varepsilon}_i$ is the computed transition energy ($\tilde{E}_i$-E) and the pseudo-oscillator strengths are defined as

$$\tilde{f}_i = 2\tilde{\varepsilon}_i |\langle \Phi | \underset{\sim}{\mu} | \chi_i \rangle|^2 \ . \tag{46}$$

The $\tilde{f}_i$ are easily accessible from the eigenvectors of a normal improved virtual orbital calculation.

E) Principal Pseudostates

The pseudostates, $\chi_i(\underline{r})$, i = 1,2,...,n, can be chosen so that 2n sequential spectral moments S(-k 1) (cf eqn. (44)) for k = 1,2,...,2n are reproduced exactly by eqn. (45), in which case they are designated as principal pseudostates. To show this, consider the linear combination,

$$\chi_i(\underline{r}) = \sum_{k=1}^{n} b_{ki}\theta_k(\underline{r}), \tag{47}$$

where the b_{ki} are chosen to satisfy eqns. (21) and (22). The $\theta_k(\underline{r})$ are given by[33]

$$\theta_k(\underline{r}) = (-1)^k [H^{(0)}(\underline{r}) - E^{(0)}]^{-k} \mu(\underline{r}) \phi^{(0)}(\underline{r}), \tag{48a}$$

$$k = 1,2,...,2n \ ,$$

where $\phi^{(0)}(\underline{r})$ is an eigenfunction of the field-free Hamiltonian, $H^{(0)}(\underline{r})$, with eigenvalue $E^{(0)}$. Equation (48a) may be rewritten in the form of a recursion relation

$$[H^{(0)}(\underline{r}) - E^{(0)}]\theta_1(\underline{r}) + \mu(\underline{r})\phi^{(0)}(\underline{r}) = 0, \tag{48b}$$

$$[H^{(0)}(\underline{r})-E^{(0)}]\theta_k(\underline{r}) + \theta_{k-1}(\underline{r}) = 0 \qquad (48c)$$
$$2 \leq k \leq 2n.$$

Thus it can be shown that the expansions

$$\phi_{\pm}^{(1)}(\underline{r}) = \sum_{k=1}^{\infty} (\pm 1)^{k+1}\theta_k(\underline{r})\omega^{k-1} \qquad (49)$$

satisfy eqn. (6) by direct substitution followed by application of the identity in eqn. (48c). From eqns. (44) and (48)[33,34]

$$S(-k+1) = (-1)^k 2\langle\phi^{(0)}|\mu|\theta_k\rangle,$$

$$k = 1,2,\ldots,2n, \qquad (50)$$

showing that $\theta_k(\underline{r})$ determines the spectral sum $S(-k+1)$. Noting that eqns. (48) are similar to the equations of static perturbation theory, it is evident that a 2n-1 theorem[35] exists such that if the function $\theta_k(\underline{r})$ is known, the sum $S(-2k+1)$ is also determined. Therefore, if the n functions $\theta_k(\underline{r})$ for $1 \leq k \leq n$ are employed as primitive basis functions in the construction of the $\chi_i(\underline{r})$ (cf eqn. (47)), the variational development will contain the correct wavefunction to $O(\omega^{n-1})$ (cf eqn. (49)), and the 2n sums $S(-k+1)$ for $1 \leq k \leq 2n$ will be reproduced exactly by eqn. (45).[36] The discrete transition frequencies and oscillator strengths $[\tilde{\varepsilon}_i, \tilde{f}_i, i = 1,\ldots,n]$ that reproduce 2n of the correct spectral sums are an optimal, or principal,

choice with reference to imaging $\alpha(z)$ for all values of complex frequency. Consequently, the primitive basis functions $\theta_k(\underline{r})$ of eqns. (48) and (49) and the linear combinations results in the pseudostates $\chi_i(\underline{r})$ of eqns. (21), (22), and (47), are designated as optimal or principal basis functions and pseudostates, respectively, in that they reproduce the principal $\tilde{\varepsilon}_i$ and $\tilde{f}_i$. From an arbitrary larger basis set of functions, n principal pseudostates can always be extracted and the principal $\tilde{\varepsilon}_i$ and $\tilde{f}_i$ values can be constructed. These latter values alone, out of all possible effective transition frequencies and oscillators constructed from a basis set of n terms, exhibit the useful properties described in Section IID, hence motivating their calculation.[37]

F) Linearization of the Moment Problem

The moment problem of Section IID is linearized through the introduction of Padé approximants[38]

$$[n,n-1](z) = P_{n-1}(z)/Q_n(z), \tag{51a}$$

$$P_{n-1}(z) = \sum_{i=0}^{n-1} a_i(n) z^i, \tag{51b}$$

$$Q_n(z) = 1 + \sum_{i=1}^{n} b_i(n) z^i, \tag{51c}$$

to the continued fration[39]

$$A(z) = \cfrac{\beta_0}{\frac{1}{z} - \alpha_1 - \cfrac{\beta_1}{\frac{1}{z} - \alpha_2 - \cfrac{\beta_2}{\frac{1}{z} - \alpha_3 - \cdots}}}$$

associated with the Stieltjes integral expanded in powers of z

$$\beta(z) = \int_{\varepsilon_1}^{\infty} \frac{\varepsilon df(\varepsilon)}{\varepsilon - z} = \sum_{k=0}^{\infty} \int_{\varepsilon_1}^{\infty} \left(\frac{z}{\varepsilon}\right)^k df(\varepsilon)$$

$$= \sum_{k=0}^{\infty} S(-k) z^k \qquad (53)$$

up to order 2n-1

$$[n,n-1](z) = \frac{1}{z}A(z) = \beta(z) = 0(z^{2n-1}). \qquad (54)$$

Equation (54) provides explicit algorithms for determining the $a_i^{(n)}$, $b_i^{(n)}$ and α_n, β_n from the moments $S(-k)$.[40] When large numbers of moments are employed it is convenient to use the recurrence relations[13]

$$Q_n(z) = (1-\alpha_n z)Q_{n-1}(z) - z^2\beta_{n-1}Q_{n-2}(z),$$

$$Q_{-1}(z) = 0 \quad , \quad Q_0(z) = 1, \qquad (55a)$$

$$P_{n-1}(z) = (1- {}_n z)P_{n-2}(z) - z\ {}_{n-1}P_{n-3}(z),$$

$$P_{-1}(z) = 0 \quad , \quad P_0(z) = \beta_0 \ , \tag{55b}$$

in constructing the polynomials $Q_n(z)$, $P_{n-1}(z)$ orthogonal with respect to the distribution $f(\varepsilon)$.[41] The α_n and β_n appearing in eqns. (52) and (55) are determined from the moments in the forms,[42]

$$\alpha_n = \frac{Y_{n-1,n}}{Y_{n-1,n-1}} - \frac{Y_{n-2,n-1}}{Y_{n-2,n-2}}, \ \alpha_o = 0,$$

$$\alpha_1 = \frac{S(-1)}{S(0)} \ , \tag{56a}$$

$$\beta_n = \frac{Y_{n,n}}{Y_{n-1,n-1}} \ , \ \beta_{-1} = 0, \ \beta_o = S(0) \tag{56b}$$

where the matrix elements

$$Y_{n,\ell} \equiv \int_o^\infty \varepsilon^{-\ell-n} Q_n(\varepsilon) df(\varepsilon) \tag{57a}$$

satisfy

$$Y_{n,\ell} = Y_{n-\ell,\ell+1} - \alpha_n Y_{n-1,\ell} - \beta_{n-1} Y_{n-2,\ell} \ , \tag{57b}$$

$$Y_{n,\ell} = 0 \ , \ \ell < n, \tag{57c}$$

$$Y_{o,\ell} = S(-\ell), \tag{57d}$$

$$Y_{n,-\ell} = Y_{-1,\ell} = 0. \tag{57e}$$

The recurrence relation (57b) is obtained directly from eqn. (55a) and the definition of eqn (57a).

Equations (56) can be written in the alternative forms

$$\alpha_n = \frac{1}{\beta_0\beta_1\cdots\beta_{n-1}}\int_0^\infty \left(\frac{1}{\varepsilon}\right)^{2n-1} Q_n(\varepsilon)^2 df(\varepsilon), \tag{58a}$$

$$\beta_n = \frac{1}{\beta_0\beta_1\cdots\beta_{n-1}}\int_0^\infty \left(\frac{1}{\varepsilon}\right)^{2n-1} Q_n(\varepsilon)^2 df(\varepsilon), \tag{58b}$$

which are particularly useful when the recurrence coefficients are to be calculated from variationally determined pseudospectra $\tilde{\varepsilon}_i$ and $\tilde{f}_i$, i = 1,...,N. In this case, eqns. (58) become

$$\tilde{\alpha}_n = \frac{1}{\tilde{\beta}_0\tilde{\beta}_1\cdots\tilde{\beta}_{n-1}} \sum_{i=1}^{N} \left(\frac{1}{\tilde{\varepsilon}_i}\right)^{2n-1} Q_{n-1}(\tilde{\varepsilon}_i)^2 \tilde{f}_i, \tag{59a}$$

$$\tilde{\beta}_n = \frac{1}{\tilde{\beta}_0\tilde{\beta}_1\cdots\tilde{\beta}_{n-1}} \sum_{i=1}^{N} \left(\frac{1}{\tilde{\varepsilon}_i}\right)^{2n-1} Q_{n-1}(\tilde{\varepsilon}_i)^2 \tilde{f}_i. \tag{59b}$$

Here the values $Q_{n-1}(\tilde{\varepsilon}_i)$ and $Q_n(\tilde{\varepsilon}_i)$ are obtained from the recurrence relations of eqns (55) using $\tilde{\alpha}_m$ and $\tilde{\beta}_m$ values of lower order than the $\tilde{\alpha}_n$ and $\tilde{\beta}_n$ being calculated.

Once the $\tilde{\alpha}_n$ and $\tilde{\beta}_n$ are determined from eqns (55) and (59) and variationally determined pseudospectra, eqns. (55) provide the polynomials $Q_n(z)$ and $P_{n-1}(z)$. The $\varepsilon_i(n)$ and $f_i(n)$ are obtained from the roots and residue of $[n,n-1](z)$ (cf. eqns. (51) - (54)) according to

$$Q_n(\varepsilon_i(n)) = 0, \tag{60a}$$

$$f_i(n) = \frac{P_{n-1}(\varepsilon_i(n))}{\varepsilon_i(n) Q_n'(\varepsilon_i(n))} . \tag{60b}$$

Finally, then we have generated a set of smoothed points and weights which determine the calculated photoionization cross section.

G) Computational Aspects

We have developed an approximate procedure for applying the Stieltjes imaging method to molecules which avoids the potentially spurious results that arise from weakly interacting spectra and also the need for extensive CI calculations to generate the pseudospectra. These approximations have been successfully tested on molecular nitrogen[19] and offer quantitatively significant simplifications in the application of the Stieltjes imaging method to molecules. In order to avoid the potentially spurious results arising from weakly interacting channels, an approximate solution of the coupled-channel problem is obtained by separating out the various physically-distinct, low-lying states of the molecular ion. Wavefunctions are constructed for these states and using these wavefunctions the ionic molecular fields in which the free electron is scattered can be defined. Each molecular ionic wave-

function determines an effective one-particle potential which reflects the nonspherical nature of the molecular core and also contains exchange effects. A set of square-integrable one-electron eigenfunctions are obtained using this potential. These eigenfunctions are then coupled to the orbitals of the core to produce dipole-allowed total molecular states which provide the discrete excitation energies and oscillator strengths, $\{\tilde{\varepsilon}_i, \tilde{f}_i\}$, that are used to construct approximate spectral moments, S(-k), and hence pseudospectra. Coupling between different ionic channels is ignored. This is equivalent to using static-exchange potentials for each ionic channel. The total photoionization cross section is just the sum of the contributions for all such channels.

In this model a set of N orbitals, ϕ_k, and hence N discrete excitation energies and oscillator strengths, is obtained from a single diagonalization of the appropriate one-particle Hamiltonian associated with the residual ion core. A final state wavefunction is of the form

$$\Psi(N) = A[\Phi_{CORE}(N-1)\,\phi_k] \tag{61}$$

where A is the antisymmetrizer, $\Phi_{CORE}(N-1)$ represents the core, and ϕ_k is a one-particle eigenfunction of the potential produced by the core. More specifically, the ϕ_k

satisfy

$$\langle\phi_j|h+V(N-1)|\phi_k\rangle = \varepsilon_k\delta_{jk} \tag{62}$$

where

$$V(N-1) = \sum_i (2a_i J_i - b_i K_i) \quad . \tag{63}$$

Here h is the kinetic energy plus nuclear attraction terms while J_i and K_i are the usual Coulomb and exchange operators. The summation goes over the orbitals of the core. The coefficients a_i and b_i are needed to specify the Coulomb and exchange potentials of the core orbitals. For closed-shell contributions or for spatially non-degenerate orbitals in unfilled shells these coefficients are simple. The proper construction of these V(N-1) potentials is important. According to eqn. (63), the $\{\phi_k\}$ are equivalent to the virtual orbitals of the V(N-1) potential. These so-called improved virtual orbitals are frequently used in bound-state molecular applications.

Our approach allows construction of the discrete pseudospectra required for the Stieltjes moment analysis from diagonalization of relatively small matrices (cf. eqn. (62)) occuring in computations with SCF Hamiltonians. In addition, there is no need to use the same set of basis functions to expand both the occupied core orbitals and the virtual orbitals ϕ_k. A modest number of valence-like basis functions with optimized orbital exponents is employed in solving for the SCF occupied orbitals. The

Hamiltonian of eqn. (62), however, is diagonalized over a much larger set of basis functions. This provides the rich spectrum required for the moment analysis. Since the augmented basis set is much larger than the basis set originally employed in the SCF calculations, only the necessary number of two-electron integrals is evaluated. If M functions are used in solving the SCF equations and N functions are used to expand the virtual orbitals, the number of two-electron integrals needed goes as $N^2 \times M^2$. In contrast, a CI calculation in this basis requires the full number of two-electron integrals ($\sim N^4$) and a transformation of these integrals which goes like N^5.

H) Illustrative Example

The energies and oscillator strengths calculated from a set of discrete pseudostates can be used to crudely approximate smooth photoabsorption cross sections without even resorting to the full machinary of the Stieltjes imaging method. We will show this to be the case for helium. The pseudostates needed for this calculation are obtained from the standard IVO computation detailed in Section III.[43]

Table I provides a set of pseudostate energies, $\tilde{\varepsilon}_i$, and oscillator strengths, $\tilde{f}_i$, for He. The $\tilde{\varepsilon}_i$ and $\tilde{f}_i$ values furnish a histogram approximation to the cumulative

oscillator strength distribution in the form

$$
\begin{aligned}
f(\varepsilon) &= 0 , && 0 \leq \varepsilon < \tilde{\varepsilon}_1 \\
f(\varepsilon) &= \sum_{i=1}^{j} \tilde{f}_i , && \tilde{\varepsilon}_j < \varepsilon < \tilde{\varepsilon}_{j+1} \\
f(\varepsilon) &= \sum_{i=1}^{n} \tilde{f}_i , && \tilde{\varepsilon}_n < \varepsilon .
\end{aligned}
\tag{64}
$$

This histogram approximation is given in Table II and Figure 1. The differential oscillator-strength distribution, $g(\varepsilon)$, is the Stieltjes derivative of eqn. (64)

$$g(\varepsilon) = \frac{df}{d\varepsilon} \approx \frac{\Delta f}{\Delta \varepsilon} , \quad \varepsilon > \varepsilon_1 \tag{65}$$

according to eqn. (12). To evaluate $g(\varepsilon)$, consider the interval between $\tilde{\varepsilon}_j$ and $\tilde{\varepsilon}_{j+1}$ in Figure 1. The midpoint of this interval is

$$\tilde{\omega}_j = \frac{1}{2}(\tilde{\varepsilon}_{j+1} + \tilde{\varepsilon}_j) \tag{66}$$

and the width of the interval is

$$\Delta\varepsilon = (\tilde{\varepsilon}_{j+1} - \tilde{\varepsilon}_j) \tag{67}$$

The change in the cummulative oscillator strength has a different value at opposite ends of the interval

$$\Delta f(\tilde{\varepsilon}_{j+1}) = \tilde{f}_{j+1} \tag{68a}$$

$$\Delta f(\tilde{\varepsilon}_{j}) = \tilde{f}_{j} \tag{68b}$$

In order to evaluate the quantity on the right side of eqn. (65) at $\tilde{\omega}_j$, we take the average of the values for Δf obtained at the right- and left-hand limits of the energy interval

$$\begin{aligned} \Delta f &= \frac{1}{2}[\Delta f(\tilde{\varepsilon}_{j+1}) + \Delta f(\tilde{\varepsilon}_{j})] \\ &= \frac{1}{2}[\tilde{f}_{j+1} + \tilde{f}_{j}]. \end{aligned} \tag{69}$$

The approximate expression for $g(\tilde{\omega}_j)$ is therefore

$$g(\tilde{\omega}_j) = \frac{1}{2}\,\frac{(\tilde{f}_j + \tilde{f}_{j+1})}{(\tilde{\varepsilon}_{j+1} - \tilde{\varepsilon}_j)} \quad . \tag{70}$$

Applying this result to the pseudostate energies and oscillator strengths listed in Table I gives the values for the differential oscillator strength in Table III. The photoionization cross section is obtained from the differential oscillator strength by utilizing the relationship of eqn. (15a) and including a factor of three to account for the spatial degeneracy of the p-wave representing

the photoejected electron. The values for the cross section are plotted in Figure 2 along with the experimental data of Samson.[44] The results of even this crude calculation turn out to be in agreement with experiment to better than 15%.

(III) CURRENT WORK

It was found that core relaxation and basis set effects caused insignificant differences in the photoabsorption cross section of N_2 calculated using the Stieltjes imaging technique.[19] The apparent insensitivity of the Stieltjes calculation to the precise nature of the required virtual orbitals led us to explore the possibility of using V(N) rather than V(N-1) potentials in computing photoionization cross sections. The motivation is convenience as well as insight into what features of the core potential have an important effect on photoionization phenomena. In general, the construction of the V(N-1) potential is considerably more involved than the construction of the V(N) potential for a particular system. Also, in obtaining the necessary virtual orbitals, the same potential is employed for all of the separate channels when dealing with the V(N) potential. When using the V(N-1) potential, however, a different potential must be constructed for each channel.

The computational procedure using the V(N) potential is similar to the procedure employed with the V(N-1) potential. An SCF calculation is performed to get the target wavefunctions. The system is then partitioned into its physically distinct channels. For each channel the original SCF basis is augmented with orbitals of the

appropriate symmetry. A virtual orbital calculation is performed using the augmented basis with the Hamiltonian chosen to represent the photoejected electron in the presence of the full V(N) potential. Care is taken to insure that the virtual orbitals constructed are orthogonal to the target orbitals.

The excitation energies must be determined for the various channel components. For example, in the case of singlet ground and final states, for an excitation between orbitals ϕ_i and ϕ_a (corresponding to a transition between states $^1\Phi_0$ and $^1\Phi_{ia}$) with orbital energies ε_i and ε_a, repectively, it can be shown[45] that

$$E(^1\Phi_{ia}) - E(^1\Phi_0) = \varepsilon_a - \varepsilon_i - (J_{ia}-2K_{ia}) \qquad (71)$$

It is noteworthy that the average excitation energy of the singlet is not what would be expected offhand, namely, $\varepsilon_a - \varepsilon_i$. The reason for this is that ε_i and ε_a are both eigenvalues of the SCF Hamiltonian of the ground state; for the excited state the quantity ε_a can therefore not be expected to have the same meaning as the orbital energies ε_i of the ground state molecular orbitals. This is known as the single-transition approximation. The matrix elements $[J_{ia}-2K_{ia}]$ are conveniently obtained by constructing the matrix representation of the operator

$[J_i - 2K_i]$ over the basis of atomic orbitals, transforming this representation to the basis of molecular orbitals, and extracting the a^{th} diagonal element of the latter matrix representation of $[J_i - 2K_i]$ to get the element $[J_{ia} - 2K_{ia}]$. It should be noted that the two-electron integrals required for this procedure are among those constructed for use in the virtual orbital calculation. To get values of $E(^1\Phi_{ia})$ from eqn. (71), $E(^1\Phi_0)$ is chosen so that the lowest value of $E(^1\Phi_{ia})$ corresponds to the appropriate experimental first Rydberg energy.

Having found the appropriate excitation energies, the transition moments, μ_{ia}, between orbitals ϕ_i and ϕ_a are calculated. The transition moments, μ_{ia}, and the corresponding excitation energies $E(^1\Phi_{ia})$, are then used to compute a set of oscillator strengths. The excitation energies and corresponding oscillator strengths serve as points and weights, respectively, for a Stieltjes moment analysis. This finally provides the partial photoionization cross section for a single channel. The sum of all of the partial cross sections yields the total photoionization cross section.

We have teseted our new approach to photoionization calculations on helium. An SCF wavefunction for the ground $^1S_0$ state of He is obtained in the basis of 10 s Gaussian functions given by Martin and McKoy.[46] For the

1s → kp transitions, 8p functions are added to the original 10s basis. The photoionization calculation was carried out using both the V(N-1) and the V(N) potential techniques.

The pseudospectra computed using the V(N-1) potential and the V(N) potential are given in Table IV. Below threshold (0.90357 au) both sets of results are considered unreliable. Above threshold the V(N) potential oscillator strengths are larger than the corresponding oscillator strengths for the V(N-1) potential but the two sets of results converge to the same values as one goes to higher energies. This behavior should be reflected in the resulting photoionization cross sections.

The photoionization cross sections obtained from the Stieltjes-Tchebyscheff moment analysis of the pseudospectra of Table IV are shown in Figures 3 and 4. The cross section calculated using the V(N) potential lies consistently above the cross section computed using the V(N-1) potential. Both calculations yield results in good qualitative agreement with the experimental work of Samson;[44] quantitatively, the cross section obtained using the V(N-1) potential is closer to experimentally determined values.

What we have concluded thus far is that photoionization cross sections in good qualitative agreement with experiment may be conveniently constructed using the

Stieltjes imaging technique where the potential in which the photoejected electron recedes is the full V(N) potential of the system. Apparently, then, the structure of the cross section is not critically dependent on the precise nature of the V(N-1) potential. We are left with the question: Why is the cross section calculated using the V(N) potential generally larger than the cross section calculated using the V(N-1) potential and the experimental cross section? We hope to be able to answer this question and apply our new approach to molecular nitrogen in the near future.

REFERENCES AND NOTES

1. R. D. Hudson, editor, "Critical Review of Ultraviolet Photoabsorption Cross Sections for Molecules of Astrophysical and Aeronomic Interest", NSRDS-NBS 38 (U.S. Govt. Printing Office, Washington, 1971).
2. F. J. Wuilleumier, editor, Photoionization and other Probes of Many-Electron Interactions (Plenum, New York, 1976).
3. a) D. R. Bates; J. Chem. Phys., 19, 1122 (1951);
   b) D. R. Bates, V. Öpik, and G. Poots, Proc. Phys. Soc. A, 66, 1113 (1953).
4. E. J. McGuire, Phys. Rev., 175, 20 (1968).
5. H. P. Kelly, Chem. Phys. Lett., 20, 547 (1973).
6. a) F. O. Ellison, J. Chem. Phys., 61, 507 (1974);
   b) J. W. Rabalais, T. P. Debies, J. L. Berkosky, J. T. J. Huang, and F. O. Ellison, J. Chem. Phys., 61, 516 (1974).
7. a) J. W. Davenport, Phys. Rev. Lett., 36, 945 (1976);
   b) D. Dill and J. L. Dehmer, J. Chem. Phys., 61, 692 (1974);
   c) J. L. Dehmer and D. Dill, Phys. Rev. Lett., 35, 213 (1975).
8. a) B. Schneider and R. S. Berry, Phys. Rev., 182, 141 (1969);
   b) H. C. Tuckwell, J. Phys. B, 3, 293 (1970);

c) S. Iwata and S. Nagukura, Mol. Phys., 27, 425 (1974);
d) C. Duzy and R. S. Berry, J. Chem. Phys., 64, 2421 (1976).

9. a) Green's function methods - M. Oppenheimer and H. Doyle, Phys. Rev. A, 13, 665 (1976);
b) Coordinate rotation methods - T. N. Rescigno, C. W. McCurdy and V. McKoy, J. Chem. Phys., 64, 477 (1976);
c) Equivalent-quadrature methods - H. A. Yamaui and W. P. Reinhardt, Phys. Rev. A, 11, 1144 (1975);
d) J-matrix methods - J. T. Broad and W. P. Reinhardt, J. Phys. B, 9, 1491 (1976).
e) Analytic continuation methods - M. A. C. Naseimento and W. A. Goddard, III, Phys. Rev. A, 16, 1559 (1977).

10. a) P. W. Langhoff, Chem. Phys. Lett., 22, 60 (1973);
b) P. W. Langhoff and C. T. Corcoran, J. Chem. Phys., 61, 146 (1974);
c) P. W. Langhoff, J. Sims, and C. T. Corcoran, Phys. Rev. A, 10, 829 (1974).

11. a) P. W. Langhoff and C. T. Corcoran, Chem. Phys. Lett., 40, 365 (1976);
b) P. W. Langhoff, C. C. T. Corcoran, J. S. Sims, F. Weinhold, and R. M. Glover, Phys. Rev. A., 14, (1976);
c) C. T. Corcoran and P. W. Langhoff, J. Math. Phys., 18, 651 (1977).

12. H. F. Schaefer III, The Electronic Structure of Atoms and Molecules (Addison-Wesley, Reading, 1972), p. 306.

13. J. A. Shohat and J. D. Tamarkin, The Problem of Moments, Mathematical Surveys; 1 (American Mathematical Society, Providence, 1943).

14. R. F. Stewart, C. Laughlin, and G. A. Victor, Chem. Phys. Lett., 29, 353 (1974).

15. P. W. Langhoff, C. T. Corcoran, and J. S. Sims, Phys. Rev. A, 16, 1513 (1977).

16. R. K. Nesbet, Phys. Rev. A, 14, 1065 (1976).

17. S. V. O'Neil and W. P. Reinhardt (submitted for publication, J. Chem. Phys.)

18. P. W. Langhoff, S. R. Langhoff, and C. T. Corcoran, J. Chem. Phys., 67, 1722 (1977).

19. T. N. Rescigno, C. F. Bender, B. V. McKoy, and P. W. Langhoff, J. Chem. Phys., 68, 970 (1978).

20. T. N. Rescigno, B. V. McKoy, and P. W. Langhoff (unpublished work)

21. P. W. Langhoff, S. T. Epstein, and M. Karplus, Rev. Mod. Phys., 44, 602 (1972).

22. a) H. Hameka, Advanced Quantum Mechanics (Addison-Wesley, Reading, 1965);
b) G. Wentzel, Z. Phys., 41, 828 (1927);
c) O. Klein, Z. Phys., 41, 407 (1927).

23. In the development of eqn.s (1) - (7), implicit use has been made of an adiabatic switching function to turn on the perturbation of eqns. (2) sufficiently slowly to ensure that eqns. (5) and (6) appropriately describe the steady state response. See Ref. 21.

24. P. M. Morse and H. Feshback, Methods of Theoretical Physics (McGraw-Hill, New York, 1953), p. 368.

25. G. V. Marr, Photoionization Processes in Gases (Academic, New York, 1967).

26. S. A. Korff and G. Breit, Rev. Mod. Phys., 4, 471 (1932).

27. By specifying a single non-degenerate symmetry we are excluding cases in which the same overall electronic symmetry can be obtained by several different couplings of photoelectron and residual ion angular moments.

28. H. F. Schaefer, Electronic Structure of Atoms and Molecules (Addison-Wesley, Reading, 1972).

29. E. J. Heller, W. P. Reinhardt and H. A. Yamani, J. Comp. Phys., 13, 536 (1973).

30. A. Ralston, A First Course in Numerical Analysis (McGraw-Hill, New York, 1965).

31. H. A. Yamani and W. P. Reinhardt, Phys. Rev. A., 11, 1144 (1975).

32. N. I. Akhieser, The Classical Moment Problem (Hafner, New York, 1965).

33. P. W. Langhoff and M. Karplus, J. Chem. Phys., 52, 1435 (1970).

34. a) P. W. Lanhoff, Chem. Phys. Lett., 9, 89 (1971); b) P. W. Langhoff, J. Chem. Phys., 57, 2604 (1972).

35. A. Dalgarno and A. L. Stewart, Proc. Roy. Soc. A, 238, 269 (1956).

36. That is, since a trial function in the form of eqn. (49) with the $\theta_k(\underline{r})$ given by eqn. (48) can reproduce the correct wavefunction to $O(\omega^{n-1})$, the variational principle ensures that it will do so. The 2n+1 theorem for time-dependent problems ensures that the resulting polarizability will be accurate to $O(\omega^{2n})$ and that the associated sum rules will be accurate for $k \leq 2n$. See S. T. Epstein, J. Chem. Phys., 48, 4716 (1968).

37. The $\theta_k(\underline{r})$ of eqns (48) can only be determined in closed form for one-electron and model systems.

38. G. A. Baker, Jr., Essentials of Padé Approximants (Academic, New York, 1975).

39. H. S. Well, Analytic Theory of Continued Fractions (Van Nostrand, New York, 1948).

40. a) R. G. Gordon, J. Math. Phys., 9, 665 (1968).
b) P. W. Langhoff and M. Karplus, Phys. Rev. Lett., 19, 1461 (1967).
c) P. W. Lanhoff and M. Karplus, J. Chem. Phys., 52, 1435 (1970).

41. It is convenient to let $x = 1/\varepsilon$ and define new polynominals $g_n(x) \equiv x^h Q_n(1/x)$ and $p_n(x) \equiv x^{(n-1)} p_{n-1}(1/x)$. See Ref. 13.

42. The Stieltjes moment theory has been used previously in the study of the dynamics of crystals lattices. See:
a) J. Deltour, Physice (Utr.), 39, 413 (1968);
b) C. Blumstein and J. C. Wheeler, Phys. Rev. B, 8, 1764 (1973).

43. A. Gerwer and V. McKoy (unpublished work)

44. J. A. R. Samson, Adv. Atomic and Molecular Physics, 2, 177 (1966).

45. T. H. Dunning and V. McKoy, J. Chem. Phys., 47, 1735 (1967).

46. P. H. S. Martin, W. H. Henneker, and V. McKoy, J. Chem. Phys., 62, 69 (1975).

TABLE I. Pseudostate Energies and Oscillator Strengths (in atomic units) for He.

$\tilde{\varepsilon}_i$	$\tilde{f}_i$
0.87653092	$0.90567709 \times 10^{-2}$
0.92263598	$0.23140472 \times 10^{-1}$
1.07249611	$0.68793441 \times 10^{-1}$
1.65871589	0.12857756×10^{0}
4.19594832	$0.702062057 \times 10^{-1}$

TABLE II. Histogram Approximation to the Cummulative Oscillator Strength for He

$\tilde{\varepsilon}$(a.u.)	$\tilde{\varepsilon}$(eV)	$\sum\tilde{f}$(a.u.)
0.87653 - 0.92264	23.852 - 25.106	$0.90567709 \times 10^{-2}$
0.92264 - 1.07250	25.106 - 29.184	$0.32197243 \times 10^{-1}$
1.07250 - 1.64872	29.184 - 40.468	0.10099068×10^{0}
1.64872 - 4.19595	40.468 - 114.179	0.22956824×10^{0}

TABLE III. Interpolated Oscillator Strength Densities and Cross Sections for He

$\tilde{\omega}_j$(a.u.)	$\tilde{\omega}_j$(eV)	g(a.u.)	σ(Mb)
0.89958345	24.479	0.34917255	8.448
0.99756605	27.145	0.30673239	7.422
1.34060600	37.024	0.17126364	4.143
2.92233211	79.522	0.03901956	0.945

TABLE IV. Pseudospectra of Transition Frequencies and Oscillator Strengths (in atomic units) for Each Channel of $(1s)^1S_0 \rightarrow (np)^1P_1$ of He.

V(N-1)		V(N)	
ω_{on}	$f_{on}/2$	ω_{on}	$f_{on}/2$
0.782824	0.425334×10^{-1}	0.779723	0.900887×10^{-3}
0.849298	0.120127×10^{-1}	0.783786	0.761726×10^{-4}
0.876531	0.905677×10^{-2}	0.791455	0.548438×10^{-2}
0.922636	0.231405×10^{-1}	0.830775	0.272770×10^{-1}
1.072496	0.687934×10^{-1}	0.980027	0.984244×10^{-1}
1.648716	0.128578×10^{0}	1.568742	0.162620×10^{0}
4.195948	0.702062×10^{-1}	4.124936	0.728655×10^{-1}
13.693166	0.412790×10^{-1}	13.622746	0.383364×10^{-2}

FIGURE CAPTIONS

Figure 1. Histogram approximation to the cummulative oscillator strength for He.

Figure 2. Photoionization cross section of He from interpolated values of the oscillator strength density.

x = values from Stieltjes theory

\+ = experimental values of Samson

Figure 3. He photoionization cross section calculated using V(N-1) potential; plus signs are calculated points; curve is fitted to experimental data of Samson.[44]

Figure 4. He photoionization cross section calculated using V(N) potential; plus signs are calculated points; curve is fitted to experimental data of Samson.[44]

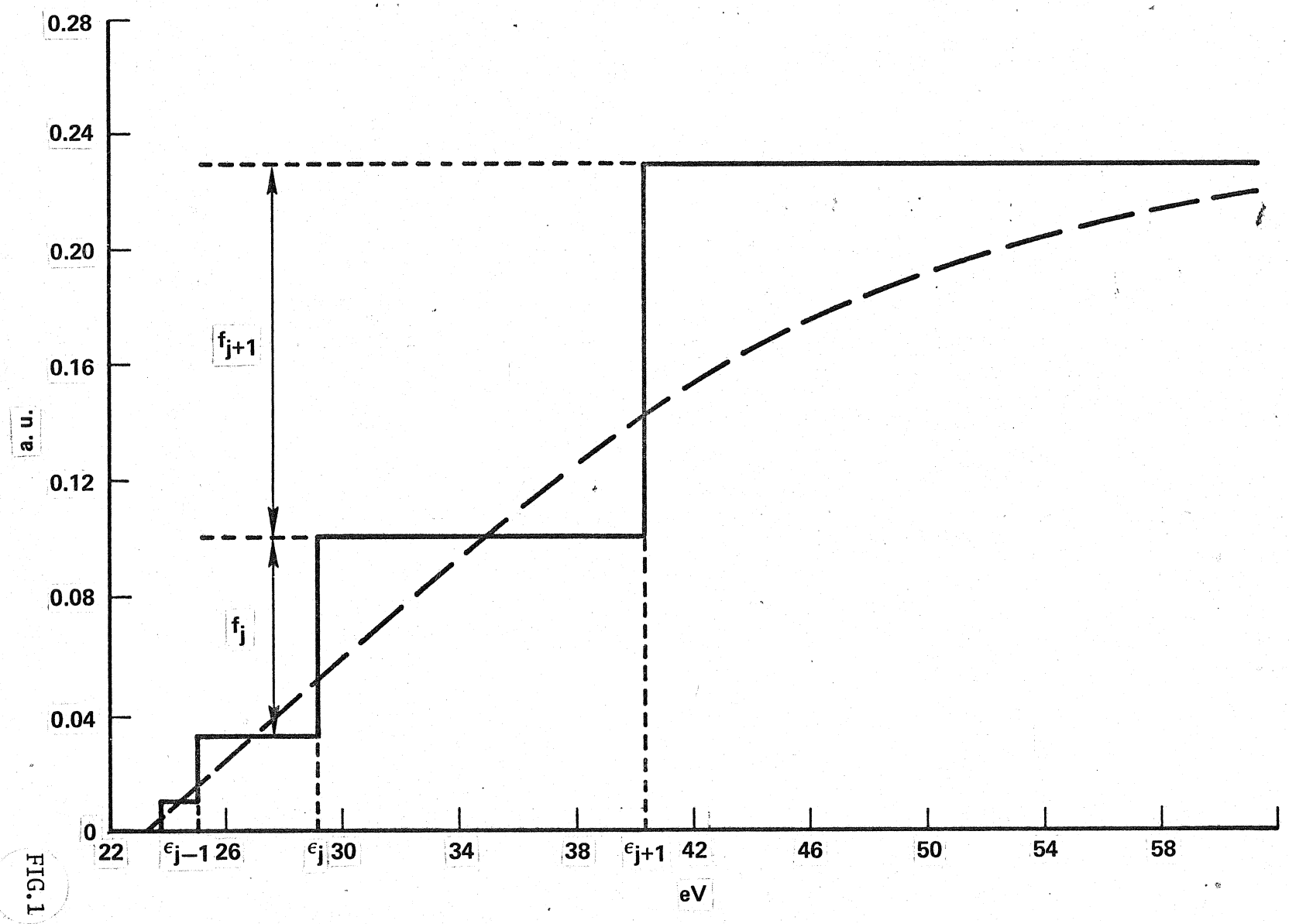
0.28
0.24
0.20
0.16
0.12
0.08
0.04
0
a. u.
f_{j+1}
f_j
22
ϵ_{j-1} 26
ϵ_j 30
34
38
ϵ_{j+1} 42
46
50
54
58
eV

FIG.1

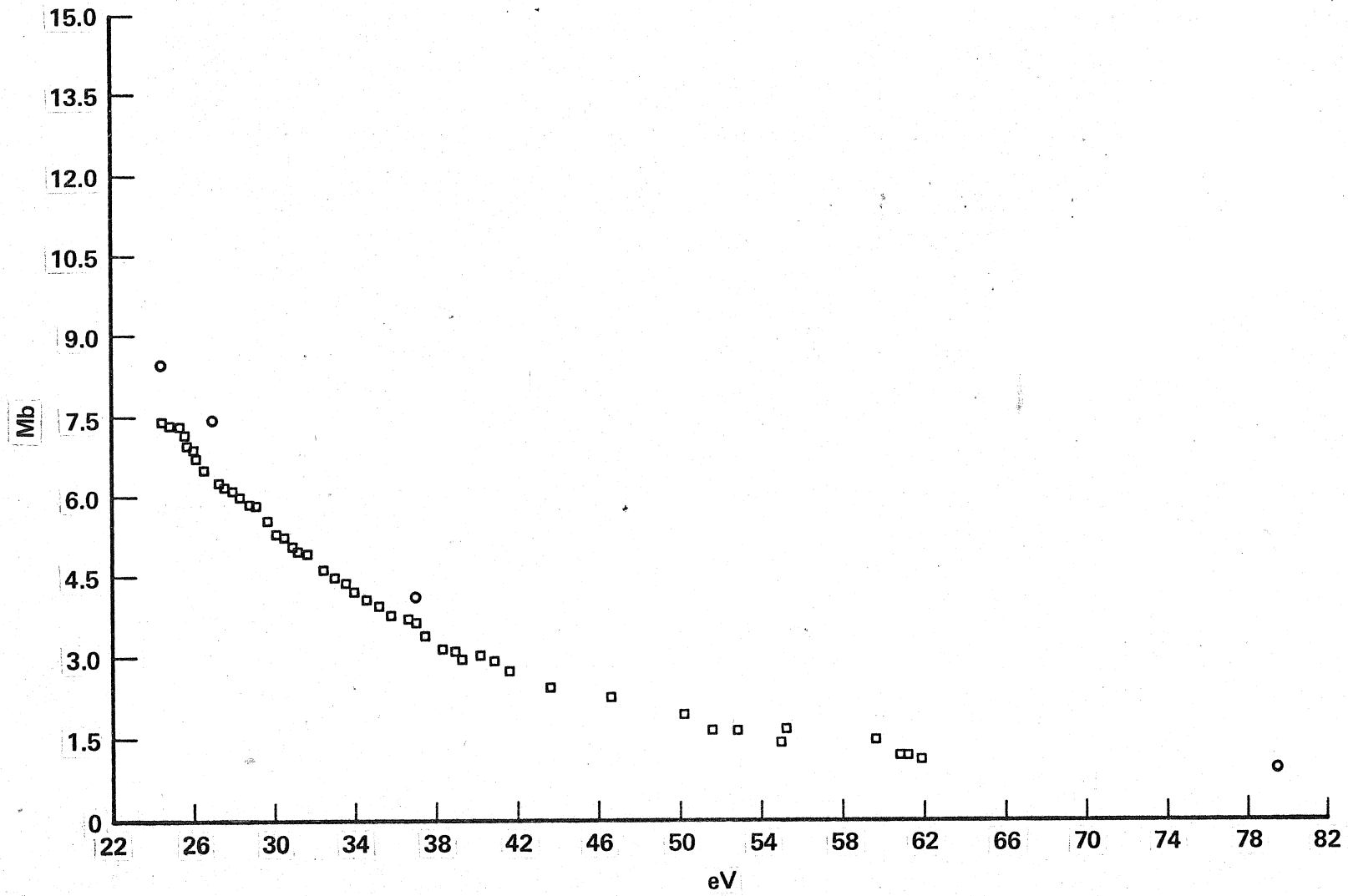
15.0
13.5
12.0
10.5
9.0
7.5
6.0
4.5
3.0
1.5
0
Mb
22
26
30
34
38
42
46
50
54
58
62
66
70
74
78
82
eV

FIG. 2

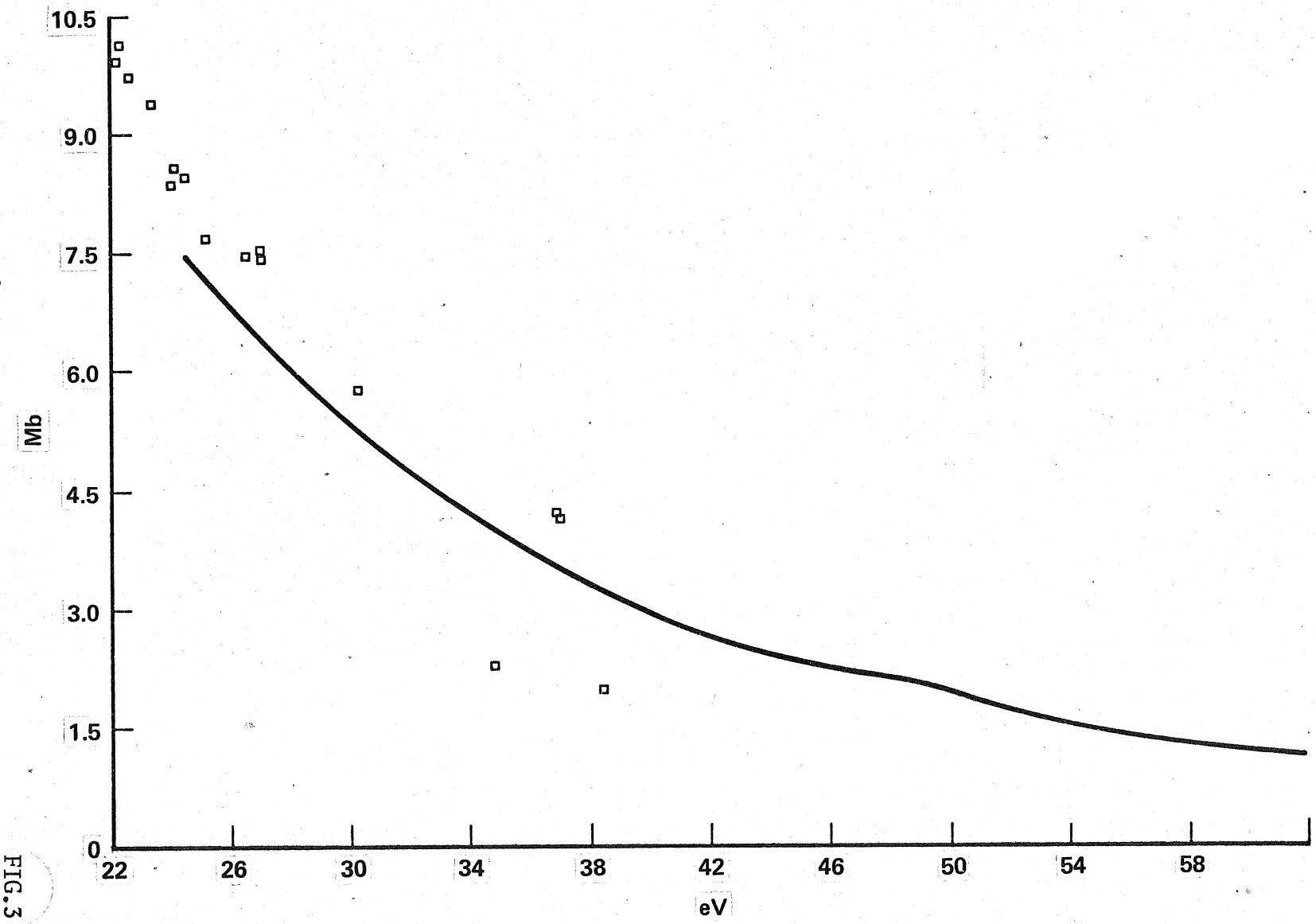

FIG.3

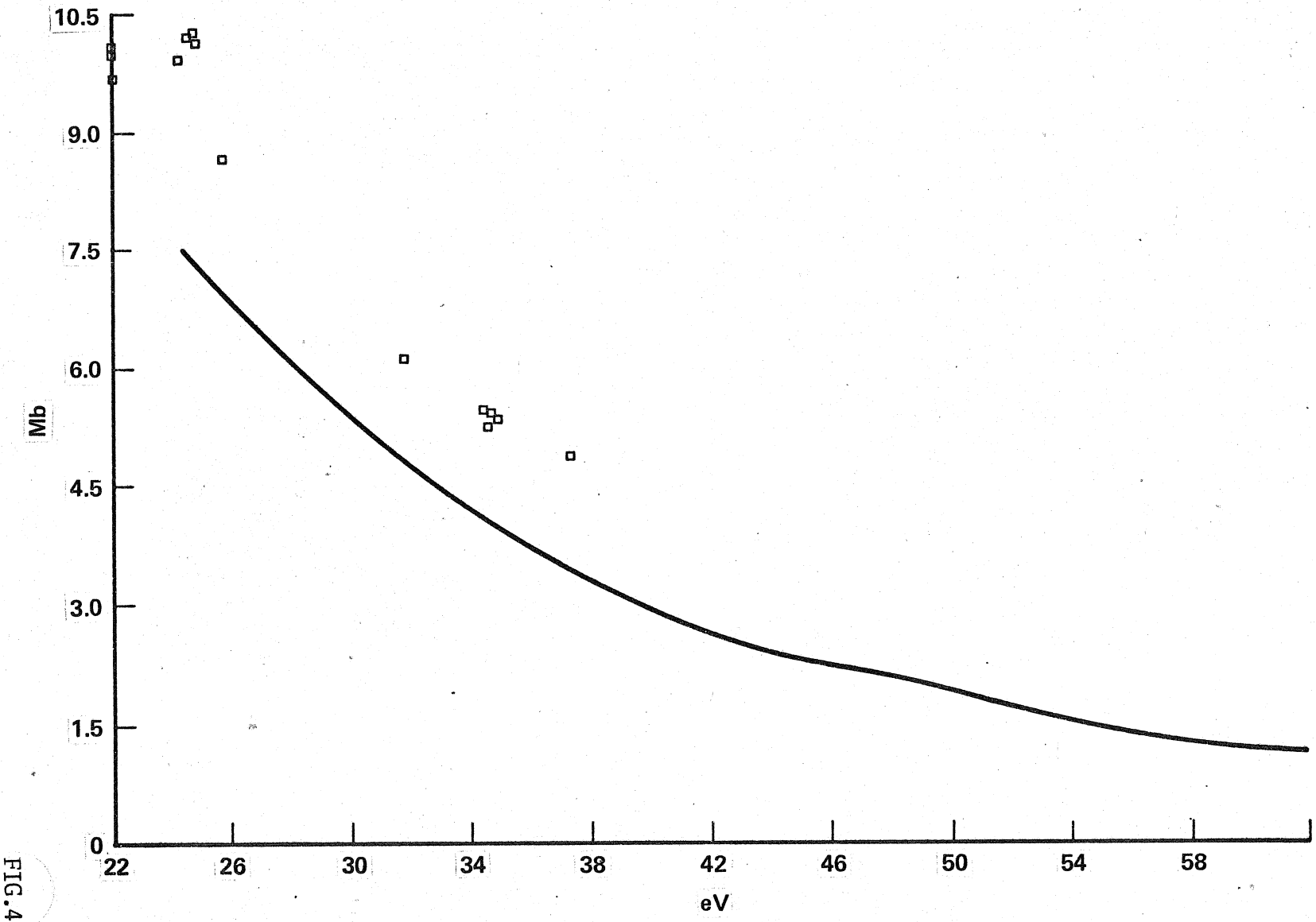

FIG.4

Appendix A

Photoexcitation and Ionization in Molecular Oxygen: Theoretical Studies of Electronic Transitions in the Discrete and Continuous Spectral Intervals.

A. Gerwer, C. Asaro, and B. V. McKoy

A. A. Noyes Laboratory of Chemical Physics,
California Institute of Technology,
Pasadena, California 91125

and

P. W. Langhoff

Department of Chemistry
Indiana University,
Bloomington, Indiana 47401

Abstract

Theoretical studies of valence-electron ($1\pi_g$, $1\pi_u$, $3\sigma_g$) photoexcitation and ionization cross sections in molecular oxygen are reported employing separated-channel static-exchange calculations and the Stieltjes-Tchebycheff moment-theory technique. As in previously reported investigations of photoexcitation and ionization in small molecules following this approach, canonical Hartree-Fock orbitals, large Gaussian basis sets, and many-electron eigenstates of correct symmetry are used in defining appropriate noncentral static-exchange potentials and in computations of the appropriate

discrete and continuum transition strengths. It is particularly important in molecular oxygen to incorporate the appropriate ionic parentages of the various photoionization multiplet states in order to obtain the correct partial-channel cross sections. The calculated discrete series associated with $1\pi_g$ excitation are found to be in good agreement with available experimental assignments and previously reported theoretical studies, and the predicted states associated with $1\pi_u$ and $3\sigma_g$ excitations are in general accord with assignments for the higher series based on spectral and quantum-defect analysis. Although the observed photoelectron spectra and photoionization cross sections are relatively complex, the calculated total vertical electronic photoabsorption cross section and the partial-channel photoionization cross sections for production of $X^2\Pi_g$, $a^4\Pi_u$, $A^2\Pi_u$, $2^2\Pi_u$, $3^3\Pi_u$, $b^4\Sigma_g^-$, and $B^2\Sigma_g^-$ ionic states are found to be in good accord with recent synchrotron radiation, line-source, electron-impact, and (e, 2e) dipole oscillator-strength measurements when proper account is taken of the parentages of the various multiplet states. The partial-channel cross sections exhibit resonance-like structures that can be attributed to contributions from diabatic valencelike virtual states that appear in the appropriate photoionization continua, rather that in the corresponding discrete spectral intervals. These features in the dipole spectrum of molecular oxygen are discussed and are contrasted and compared with the results of previously reported related studies in molecular nitrogen and carbon monoxide.

I. INTRODUCTION

Recently reported theoretical[1-6] and experimental[7-14] photoexcitation and ionization studies reveal the presence of resonancelike features in certain of the partial-channel photoionization cross sections of diatomic (N_2, CO) and polyatomic (H_2O,H_2CO) molecules. Elementary qualitative arguments suggest these resonance features can be attributed to contributions to the cross sections from σ^* and other valencelike virtual orbitals that appear in the appropriate photoionization continua, rather than in corresponding discrete spectral intervals. To achieve quantitative agreement with the measured outervalence-shell partial-channel cross sections, it is apparently sufficient to employ the static-exchange approximation and noncentral molecular potentials in the calculations. Appropriately chosen local noncentral potentials can also reproduce some of the general features of the spectra,[15,16] although simpler approximations involving, for example, plane-wave[17] and one- and two-center[18,19] Coulombic final states generally lead to qualitatively incorrect cross sections that can be an order of magnitude or more in error. In view of the fundamental importance of resonances in molecular photoionization continua to our understanding of electronic excitation/ionization spectra and their molecular-orbital interpretations, and in light of continuing line-source, synchrotron and bremsstrahlung

radiation, electron-impact, and (e, 2e)/(e, e+ion) coincidence studies of dipole processes in small molecules, further quantitatively reliable theoretical investigations of appropriately chosen systems are clearly in order.

The photoabsorption spectrum of molecular oxygen has been the subject of continuing experimental and theoretical interest, as a partial consequence of its importance in atmospheric and related photochemistry.[20] In spite of a great many previous theoretical and experimental investigations,[21] the general features of the oxygen continuous spectrum have been experimentally established comparatively recently,[22-28] and the reported corresponding theoretical studies do not particularly clarify the observed results. In the present study, outer-valence-shell electronic photoexcitation and ionization cross sections in molecular oxygen are obtained in the separated-channel static-exchange approximation employing the previously devised Stieltjes-Tchebycheff (S-T) moment-theory technique and L^2 variational methods.[29-32] As in previously reported studies of photoexcitation and ionization employing this approach,[1-6] Hartree-Fock canonical orbitals and Gaussian basis functions are used in molecular oxygen in calculating one-electron discrete excitation series and continuum pseudostate spectra, and many-electron eigenstates of correct symmetry are employed in calculations of appropriate transition strengths. Particular care must be exercised in properly incorporating the ionic parentages

of the various multiplet photoionization states in order to obtain the correct partial-channel cross sections in molecular oxygen. Excitations of the $1\pi_g$, $1\pi_u$, and $3\sigma_g$ outer valence orbitals are considered, whereas studies of the $2\sigma_g$, $2\sigma_u$ inner-valence and $1\sigma_g$, $1\sigma_u$ K-shell orbitals are described in separate reports. The calculated discrete series converging on the ground $(1\pi_g^{-1})X^2\Pi_g$ molecular ionic state are found to be in generally good agreement with experimental assignments and previously reported theoretical values, in spite of the use of a frozen core and the single-configurational approximation. Although the predicted positions of the higher $1\pi_u$, $3\sigma_g$ excitation series are in general accord with assignments made on basis of spectral and quantum-defect analysis, definitive studies in these regions will require appropriate autoionizing line-shape calculations not reported here. The calculated partial-channel cross sections for the production of $X^2\Pi_g$, $a^4\Pi_u$, $A^2\Pi_u$, $2^2\Pi_u$, $3^2\Pi_u$, $b^4\Sigma_g^-$ and $B^2\Sigma_g^-$ ionic states are found to be in good accord with recent line-source[25] and (e, 2e)[28] dipole oscillator-strength measurements. Similarly, the calculated total photoabsorption/ionization cross section is found to be in good accord with the results of recent electron impact,[22,28] continuum and line source,[23-26] and (e, e+ion)[28] dipole oscillator-strength measurements. Although the measured photoelectron spectra and corresponding partial-channel and total photosbsorption/ionization cross sections in molecular oxygen are relatively complex, the

static-exchange approximation is seen to account satisfactorily for the observed results, provided proper cognizance is taken of the parentages of the various multiplet states. Moreover, a previously unassigned band in the photoelectron/ionization spectrum is assigned on the basis of the present investigation. Resonance features appearing in certain of the individual channel components are attributed to contributions to the cross sections from valencelike diabatic states appearing in the corresponding photoionization continua. Specifically, compact $\sigma_\mu 2p, \pi_\mu 3p, \pi_\mu 3d, \delta_g 3d$, and $\delta_u 3d$ orbitals apparently contribute to the $1\pi_g^{-1}$, $1\pi_\mu^{-1}$, and $3\sigma_g^{-1}$ valence photoionization channels, rather than to the corresponding discrete spectral intervals. These and other features of the molecular oxygen spectrum are discussed, and are contrasted and compared with the results of related previously reported theoretical investigations of dipole excitation/ionization spectra in molecular nitrogen and carbon monoxide.[1-3]

A brief description of the Stieltjes-Tchebycheff technique in the separated-channel static-exchange approximation is given in Sec. II, the calculation required in molecular oxygen are summarized in Sec. III, and the resulting photoexcitation and ionization cross section are reported in Sec. IV. A summary discussion of the resonance features is provided in Sec. V and concluding remarks are made in Sec. VI.

II. THEORETICAL APPROACH

The Stieltjes-Tchebycheff procedure and the separated-

channel static-exchange approximation are described in considerable detail in previous publications.[1-6,29-32] Consequently, it is sufficient here to provide a brief heuristic description of the general scheme, and to refer the reader to earlier reports for further details.

A ground-state Hartree-Fock function is first constructed near the equilibrium molecular geometry employing Gaussian basis orbitals and appropriate computational methods.[33,34] Many-electron eigenstates of correct parentage and symmetry are employed in constructing noncentral static-exchange potentials for each orbital excitation considered from the occupied canonical orbitals, and corresponding one-electron Schrodinger equations are formed for the calculation of excitation spectra. The one-electron equations are solved variationally employing significantly larger basis sets than that used in constructing the ground-state Hartree-Fock function. A considerable reduction in computational effort is achieved by noting that only a subset of two-electron integrals, involving two basis orbitals from the occupied valence space and two from the supplemental or virtual space, is required in constructing variational solutions.[1,2] The one-electron eigenvalues obtained that are below the occupied-orbital ionization potential, and the corresponding one-electron orbitals, provide approximations to the appropriate discrete or autoionizing valence and Rydberg states. Those eigenvalues above the ionization potential, and their corresponding orbitals, provide pseudospectra for the Stieltjes-

Tchebycheff moment analysis, from which the appropriate photoionization cross sections are obtained. The necessary excitation and ionization transition strengths are constructed from many-electron eigenstates of correct parentage and symmetry. It is important to note that in order for the S-T analysis to be satisfactory, and to provide the correct static-exchange photoionization cross sections, it is necessary that the calculated pseudospectra correctly describe the appropriate continuum eigenstates over the finite regions of space.

The S-T approach employs a pseudospectrum of discrete transition frequencies and oscillator strengths, calculated in the present study as indicated above, in a smoothing procedure in which a continuous approximation to the underlying photoionization cross section is obtained. Conventional spectra power moments, which are convergent in the L^2 pseudospectrum of energies and strengths,[35] are generally regarded as intermediaries in the smoothing procedure, providing a basis for establishing the convergence of the overall procedure. In actual calculations, however, the power moments are avoided, and a highly stable computational algorithm is employed in constructing so-called recurrence coefficients, and moment-theory spectra of (principal) frequency points and weights, directly from the quantum-mechanically determined pseudospectrum.[29-32] The moment-theory spectra exhibit useful properties which the original pseudospectrum does not exhibit, and, in particular, provide bounds on the cumulative oscillator-strength distribution. The latter can be differentiated in

a variety of ways to provide a final expression for the photoionization cross section. Stieltjes derivatives of various orders are generally employed to obtain a first approximation to the continuous cross section, and to establish the range of convergence of the variationally calculated recurrence coefficients. Tchebycheff derivatives and appropriate recurrence-coefficient extention procedures are then used to construct a continuous approximation to the cross section. Alternatively, specific analytic forms fit to the cumulative Stieltjes histograms provide expressions convenient for differentiation. Previous investigations indicate the method is highly satisfactory, provided that the quantum-mechanical pseudostate calculation contains sufficient information pertaining to the underlying continuous spectrum.[1-6]

It is perhaps appropriate to note that the S-T approach to photoionization is not limited to the separated-channel static-exchange approximation employed here. Coupled-channel static-exchange calculations, for example, can also be performed employing generally available computer codes. Since a number of static ionic cores are employed in this approach, well-defined total and partial-channel cross sections are obtained directly from the calculations. By contrast, when correlated ground-state functions and polarized or relaxed final-state core functions are employed, special projection or related procedures--which have yet to be clarified fully --are required in determining the pseudospectra corresponding to specific photoionization channels. Moreover, the necessary quantum-mechanical calculations, of course, become somewhat

more elaborate when correlated ground-state and ionic core functions are employed. In order to gain further experience with the S-T approach to molecular photoionization, and to clarify the general natures of molecular photoionization cross sections, it is perhaps appropriate to investigate members of the large class of molecules for which the static-exchange approximation is suitable. This class should include those molecules in which photoelectron spectra are well described by the orbital approximation and Koopmans' theorem, and in which the effects of shake up and rearrangement are small. Although the observed valence photoelectron[36-38] and photoionization[25-28] spectra in molecular oxygen are relatively complex, it will be seen that the static-exchange approximation accounts satisfactorily for the measured results provided proper cognizance is taken of the ionic parentages of the various multiplet states. Relaxation and related effects are presumably of more consequence in the inner-valence and core spectra, however.[22-24]

III. MOLECULAR OXYGEN CALCULATIONS

The electronic ground state of molecular oxygen is written in the Hartree-Fock approximation in the symbolic form

$$(1\sigma_g^2 1\sigma_\mu^2 2\sigma_g^2 2\sigma_\mu^2 3\sigma_g^2 1\pi_\mu^4 1\pi_g^2) X^3\Sigma_g^- \quad , \qquad (1)$$

where the indicated canonical orbitals are obtained in the conven-

tional manner.[33,34] In the present calculations a (10s,5p,1d)/[3s, 2p, 1d] contracted Gaussian basis set is employed at $R_e = 2.282a_o$, giving a total SCF energy of -149.634 a.u.,[34] compared with the H-F limit of -149.666 a.u.[39]

The types of one-electron excitation and ionization series considered here can be written in the symbolic forms

$$(1\pi_g^{-1}k\sigma_u)^3\Pi_u \quad , \quad (1\pi_g^{-1}k\pi_u)^3\Sigma_u^- \quad , \quad (1\pi_g^{-1}k\delta_u)^3\Pi_u, \qquad (2a)$$

$$(1\pi_u^{-1}k\sigma_g)^3\Pi_u \quad , \quad (1\pi_u^{-1}k\pi_g)^3\Sigma_u^- \quad , \quad (1\pi_u^{-1}k\delta_g)^3\Pi_u, \qquad (2b)$$

$$(3\sigma_g^{-1}k\sigma_u)^3\Sigma_u^- \quad , \quad (3\sigma_g^{-1}k\pi_u)^3\Pi_u \quad , \qquad (2c)$$

where excitations of the $2\sigma_g$, $2\sigma_u$ and $1\sigma_g$, $1\sigma_u$ orbitals, which remain doubly occupied, are not considered. There are, consequently, eight distinct individual channels for excitation of the $3\sigma_g$, $1\pi_u$, and $1\pi_g$ orbitals, three corresponding to $^3\Sigma_u^-$ symmetry, and five to $^3\Pi_u$ symmetry. However, because of the open $1\pi_g$ shell in O_2 some of the eight channels are comprised of two or more subchannels associated with the formation of various distinct parent molecular O_2^+ ions. Appropriate many-electron pseudospectral wave functions and corresponding static-exchange potentials must be constructed for each of these subchannels.

In the case of excitation and ionization of the outermost $1\pi_g$ orbital [Eq. (2a)], the resulting core configuration gives rise to only the ground $X^2\Pi_g$ molecular O_2^+ ionic state.

Consequently, in this case three appropriate sets of many-electron pseudospectral functions and three corresponding static-exchange potentials must be constructed to describe the excitation and ionization of $1\pi_g$ electrons into $k\sigma_u$, $k\pi_u$, and $k\delta_u$ orbitals, respectively. In the case of excitation and ionization of the $1\pi_u$ orbital [Eq. (2b)], however, the remaining $1\pi_u^3 1\pi_g^2$ core configuration gives rise to five separate electronic molecular ionic states. Of these, two [$a^4\Pi_u$, $^2\Pi_u(1)$] arise from the ground-state $(1\pi_g^2)\,^3\Sigma_g^-$ parent, whereas three [$^2\Phi_u$, $^2\Pi_u(2)$, $^2\Pi_u(3)$] arise from the excited-state $(1\pi_g^2)\,^1\Sigma_g^+$ and $(1\pi_g^2)\,^1\Delta_g$ parents. As a consequence of the frozen-core approximation inherent in the static-exchange approach, only the $a^4\Pi_u$ and $^2\Pi_u(1)$ ionic states contribute to dipole transitions in molecular oxygen, since these arise from the $(1\pi_g^2)\,^3\Sigma_g^-$ parent. However, approximations to the spectroscopically observed $A^2\Pi_u$, $2^2\Pi_u$, and $3^2\Pi_u O_2^+$ states[40] are formed from linear combinations of the $^2\Pi_u(1)$, $^2\Pi_u(2)$, and $^2\Pi_u(3)$ static-exchange states in the present development. Consequently, four parent O_2^+ ionic states [$a^4\Pi_u$, $A^2\Pi_u$, $2^2\Pi_u$, $3^2\Pi_u$] can be produced on basis of the static-exchange approach upon excitation and ionization of a $1\pi_u$ electron. Strictly speaking, it is necessary to construct distinct $1\pi_u \rightarrow k\sigma_g$, $k\pi_g$, $k\delta_g$ orbital pseudospectra corresponding to each of these four separate ionic states. However, in accordance with the approximations inherent in multiplet theory, virtual orbitals are chosen here in a democratic fashion to be appropriate for all the states arising from $1\pi_u^3 1\pi_g^2 k\sigma_g$, $1\pi_u^3 1\pi_g^2 k\pi_g$, and $1\pi_u^3 1\pi_g^2 k\delta_g$ configurations. In this way only three distinct orbital pseudospectra are required in forming the 12 many-electron pseudospectra associated with the four parent O_2^+ ionic states formed upon excitation and ionization of a $1\pi_u$ electron. In the case of $3\sigma_g$ excitations [Eq. (2c)], the $3\sigma_g 1\pi_g^2$ configuration gives rise to $b^4\Sigma_g^-$, $B^2\Sigma_g^-$, $^2\Sigma_g^+$, and

$C^2\Delta_g$ final O_2^+ ionic states. Of these, only $b^4\Sigma_g^-$ and $B^2\Sigma_g^-$, which arise from the $(1\pi_g^2)^3\Sigma_g^-$ ground-state configuration, contribute to the molecular oxygen excitation and ionization spectra in the static-exchange approximation. As in the case of the $1\pi_u$ orbital, democratically chosen $k\sigma_u$ and $k\pi_u$ orbitals appropriate for both ionic states are employed in constructing many-electron wave functions for $3\sigma_g$ excitation and ionization. More refined calculations in which orbitals associated with specific final ionic states are employed can, of course, also be performed. It is found, however, that the pseudospectral orbitals are relatively insensitive to these refinements, and, consequently, democratically chosen orbitals are employed here.

In each of the eight individual cases [Eqs. (2)], the appropriate one-electron Schrödinger equations are written as

$$(h_\Gamma - \varepsilon)\phi_{\Gamma,\varepsilon} = 0 \quad , \tag{3}$$

where ε corresponds to continuum or discrete energies, and

$$h_\Gamma = T + V + V_\Gamma \tag{4}$$

is the static-exchange Hamiltonian, with T and V the kinetic and nuclear-framework-potential energy operators, and V_Γ the appropriate nonlocal channel potential. The nonlocal molecular channel potentials V_Γ are all written in the forms

$$V_\Gamma = \sum_i 2a_i^\Gamma J_i - b_i^\Gamma K_i \quad , \tag{5}$$

where J_i and K_i are the familiar orbital Coulomb and exchange operators,[33] and the coefficients a_i^Γ, b_i^Γ must be determined in each case. Explicit expressions for the latter, based on a previously reported analysis of open shell SCF energy expressions,[41] are given in Table I. It is perhaps helpful to note in this connection that the static-exchange calculations give results identical with dipole spectra obtained from appropriate single-excitation configuration-interaction calculations in which Hartree-Fock ground-state canonical orbitals are used to describe the frozen final-state core configurations.[42] Consequently, the open-shell static-exchange potentials of Table I are obtained simply by including in the appropriate energy functionals multiplicity weighted contributions from all linearly independent eigenstates of correct symmetry that can be formed by coupling the photo-excited final-state orbitals with the appropriate static core states indicated above.

In order to obtain useful variational solutions of Eq. (3) in each case, it is necessary to use relatively large basis sets of Gaussian orbitals. This large-basis-set requirement is a partial consequence of the structure of Cartesian Gaussian functions, which exhibit only the minimum number of nodes for each orbital angular momentum considered. Fortunately, it is not necessary that the variational solutions reproduce in detail the oscillatory behaviors of scattering functions over large regions of space in order to obtain reliable photoionization cross sections, since the product of dipole moment operator and ground state orbital provides a finite box in which the final-state function must be determined.[32] Even with this helpful simplification, however, it is generally necessary to expand the basis sets employed to the limit of linear dependence in order to obtain fully converged results.

In Table II are shown the supplemental basis functions employed in the present study in addition to the valence basis used in construction of the ground-state Hartree-Fock function.[34] The variational solutions of Eq. (3) obtained in this extended basis correspond to pseudospectra of $23\sigma_g$, $23\sigma_u$, $16\pi_g$, $16\pi_u$, $13\delta_g$, and $9\delta_u$ orbitals. As a convenience in evaluating the appropriate transition integrals, the solutions of Eq. (3) are explicitly orthogonalized to the occupied canonical Fock orbitals. Past experience indicates this generally has small effect on the calculated cross sections relative to results obtained without the explicit orthogonality constraint. In the case of molecular oxygen, however, there is a somewhat more significant effect in that the $1\pi_u \rightarrow 1\pi_g$ transition is excluded from the calculation by the orthogonality constraint. Since this excitation in the static-exchange approximation corresponds to the well-known $X^3\Sigma_g^- \rightarrow B^3\Sigma_u^-$ Schmann-Runge bands,[40] however, it is not necessary to explicitly add the appropriate vertical energy and f number to the spectrum in this case.

As in the previously reported studies in this series,[1-3] one-electron transition energies and oscillator strengths

$$\tilde{\varepsilon}_i^\Gamma = \varepsilon_\Gamma + \varepsilon_i^\Gamma \quad , \tag{6a}$$

$$\tilde{f}_i^\Gamma = (2/3)\tilde{\varepsilon}_i^\Gamma |< \phi_i^\Gamma |\vec{\mu}| \phi_\Gamma > |^2 \tag{6b}$$

are formed using experimental, rather than Koopmans, adiabatic ionization potentials ε_Γ,[36-38] thereby insuring convergence to the appropriate series limits, and allowing in some measures for the effects of core relaxation. When the one-electron pseudospectra of Eqs. (6) are determined

for the eight individual channels of Eqs. (2) to (5) and Table I, it only remains to determine the total line strengths associated with each of the many-electron final states.[43,44] These provide the many-electron pseudospectra of transition frequencies and multiplet oscillator strengths associated with the production of specific parent molecular O_2^+ ionic states.

The foregoing analysis indicates that the static-exchange approach to valence-electron ($1\pi_g$, $1\pi_u$, $3\sigma_g$) photoionization in molecular oxygen predicts the appearance of seven distinct ionic states [$a^4\Sigma_u^-$, $A^2\Pi_u$, $b^4\Sigma_g^-$, $X^2\Pi_g$, $B^2\Sigma_g^-$, $2^2\Pi_u$, $3^2\Pi_u$] in the photoelectron spectra. These are all observed in the (e, 2e) experiments,[28] although some of the states are not separately resolved. Higher resolution lower-energy line-source measurements [25,36-38] are helpful in these cases in separating the unresolved (e, 2e) data. The additional ionic states observed in the (e, 2e) spectra [$c^4\Sigma_u^-$, $^2\Sigma_u^-$, $^{2,4}\Sigma_g^-$] can be attributed to $2\sigma_u$ and $2\sigma_g$ photoionization not treated here, with the exception of the $c^4\Sigma_u^-$ state, which is a well-known two-electron excitation.[45] The latter contributes weakly to the photoelectron and ionization spectra, however, and, consequently, the static-exchange approximation apparently accounts for all the important features of the valence-shell measurements.

IV. PHOTOEXCITATION AND IONIZATION CROSS SECTIONS IN MOLECULAR OXYGEN

In Tables III-V and Figs. 1-4 are shown the discrete excitation series and photoionization cross sections, respectively, obtained from the present calculations. These results are discussed in detail in the following subsections. In order to obtain some preliminary qualitative indication of the natures of the spectra, it is perhaps helpful to re-

call that both compact and diffuse virtual molecular orbitals are anticipated in the excitation spectrum of molecular oxygen on basis of elementary considerations.[46,47] Specifically, a valencelike $\sigma_u 2p$ or σ^* virtual orbital is expected to participate in strong $N \rightarrow V_\sigma$ excitations in the molecular oxygen spectrum, and strong $N \rightarrow V_\pi$ transitions into the valencelike $1\pi_g$ or π^* orbital are also expected on this basis, since this shell is partially open. In addition to the presence of these predominantly valencelike σ^* and π^* orbitals, previous experience suggests the appearance of certain partially valence or pre-Rydberg $\delta_g 3d$, $\delta_u 3d$, $\pi_u 3p$, and $\pi_u 3d$ orbitals,[48] and appropriate discrete and continuum Rydberglike orbitals, in the molecular oxygen excitation/ionization spectra.[1-6]

Although the foregoing qualitative concepts are suggestive, the quantitative details of photoexcitation and ionization cross sections must, of course, be determined by appropriate calculations. In particular, the contributions of strong intravalence transitions to the discrete or continuous spectra are expected to be quite sensitive to the details of the calculations and, consequently, relatively large basis sets are required to obtain the correct separated-channel static-exchange results. Previous experience indicates that the valencelike orbitals indicated above can contribute substantially to the continuous spectra in first row diatomics.[1-6]

A. $1\pi_g$ spectra (I.P. = 12.1 eV)

In Table III and Fig. 1 are shown the results of the present calculations for $1\pi_g$ excitation and ionization, respectively. Referring to Table II, it is seen that $23\sigma_u$, $16\pi_u$, and $9\delta_u$ pseudospectra are used in calculating $1\pi_g$ excitation and ionization cross sections. As indicated

in the preceding section, the various Rydberg series are made to converge on the experimentally observed $X^2\Pi_g O_2^+$ adiabatic ionization potential.[36-38] The predicted $1\pi_g \rightarrow n\pi_u$ excitation series is evidently in good agreement with the positions and intensities of the observed $np\pi_u$ series,[21,49-51] and the first three members of the series are essentially identical with the earlier IVO calculations.[50] The position of the n = 3 member of this series, corresponding to excitation into a $3p\pi_u$ Rydberg orbital ($n^* \sim 2.2$, $\delta \sim 0.8$), is taken from the recent electron impact-excitation measurements.[50] The effective principle quantum number (2.2) of the resonance transition substantiates the $3p\pi_u$ assignment, since Rydberg p-orbital quantum defects for the first row diatomics are generally ~0.6 to 0.8.[51] Of course the present calculation neglects the Rydberg-valence interaction between the $(1\pi_g^{-1}3p\pi_u)^3\Sigma_u^-$ and $(1\pi_u^{-1}1\pi_g)^3\Sigma_u^-$ configurations, which apparently results in a shift of ~0.4 eV in the position of the first Rydberg state.[52-54]

In addition to the discrete Rydberg $np\pi_u$ states in O_2 indicated above, relatively compact pre-Rydberg atomic oxygen 3p and 3d orbitals (Table II) can also contribute to the $1\pi_g \rightarrow k\pi_u$ photoabsorption spectrum.[48] Referring to Fig. 1(a), a very broad and strong resonancelike $\pi_u 3d$ feature is evidently present in the $1\pi_g \rightarrow k\pi_u$ photoionization cross section, having a maximum at ~28 eV. An oxygen d-orbital interpretation of this feature is consistent with earlier theoretical studies, which indicate that compact $\pi_u 3d$ oxygen orbitals do not contribute significantly to the discrete $1\pi_g \rightarrow n\pi_u$ excitations in molecular oxygen.[50] However, since a very large Gaussian basis set is employed in the present calculation, it is not possible to unambiguously assign the qualitative nature of this resonancelike feature by inspection of the appropriate IVO orbital vec-

tors. Single-center expansions or computer plots of the resonancelike orbitals, which are not presented here, would provide useful information and are the subject of subsequent investigations. Moreover, diabatic calculation on configurational states of the type $(1\pi_g^{-1}\pi_u 3d)^3\Sigma_u^-$ and $(1\pi_g^{-1}\pi_u 3p)^3\Sigma_u^-$ would also be helpful in this connection.

The $1\pi_g \rightarrow n\sigma_u$ excitation series shown in Table III is evidently in good agreement with the experimental assignments and previous IVO calculations.[49,50] Since the low-lying state at ~8.5 eV has such a small f number it is not observed experimentally. The nature of this state, and of the entire $1\pi_g \rightarrow n\sigma_u/k\sigma_u$ spectrum, is clarified by inspection of the appropriate potential curves,[54] which indicate a diabatic $(1\pi_g^{-1}\sigma_u 2p)^3\Pi_u$ state crosses the $(1\pi_g^{-1}np\sigma_u)^3\Pi_u$ Rydberg series almost vertically in the neighborhood of the $X^3\Sigma_g^-$ equilibrium internuclear separation. Rydberg-valence interaction results in the weak low-lying transition at ~8.5 eV, with the diabatic intensity spreading over the higher Rydberg states and into the photoionization continuum. Indeed, there is evidence of a weak resonancelike $1\pi_g \rightarrow \sigma_u 2p$ contribution just above threshold in the $1\pi_g \rightarrow k\sigma_u$ photoionization cross section of Fig. 1(a). This interpretation is also consistent with recent valence-basis CI calculations in O_2, which locate the $1^3\Pi_u$ state at ~11 eV,[55] although inspection of the appropriate vector is required to confirm this assignment. Interaction of the diabatic valence state with diffuse basis functions, not included in the CI calculations,[55] presumably gives rise

to the small shift to higher energy obtained from the present study. The second state in the $1\pi_g \rightarrow np\sigma_u$ series is perturbed but clearly Rydberg in nature with principle quantum n = 3 and quantum defect $\delta \cong 0.5$. Evidently, the calculated f numbers for the series are not entirely in accord with the approximate experimental intensity designation, a discrepancy that can be attributed to the sensitivity of transition strengths to Rydberg-valence interactions.

The $1\pi_g \rightarrow n\delta_u$ series of Table II is evidently weak, accounting for the lack of an experimental assignment in this case. Those values listed under "previous calculation" in Table III in this case are obtained from the Rydberg formula for n = 3 and 4 employing a quantum defect of 0.1,[51] as is indicated in the table. The corresponding effective principle quantum numbers of 2.9 and 3.9 are in poor accord with the calculated IVO values of 3.55 and 4.93, suggesting that a compact $\delta_u 3d$ orbital contributes only weakly to the discrete $1\pi_g \rightarrow n\delta_u$ excitation series. However, referring to Fig. 1(a), a 3d pre-Rydberg atomic oxygen orbital can be regarded as contributing strongly to the $1\pi_g \rightarrow k\delta_u$ photoionization continuum at ~28 eV, since Table II indicates that the $k\delta_u$ final-state resonance feature can only be due to atomic oxygen d orbitals. It is of particular interest to note that the peak in the cross section in this case is identical with that in the $1\pi_g \rightarrow k\pi_u$ profile, substantiating in some measure the 3d atomic oxygen character of both features (Table II). Diabatic calculations on the $(1\pi_g^{-1}\delta_u 3d)\,^3\Pi_u$ configurational

state would be helpful in this connection.

Since the potential energy curve of the $X^2\Pi_g O_2^+$ state is deep and situated approximately vertically above the $X^3\Sigma_u^- O_2$ ground state,[40] the Franck-Condon factors favor only a few low-lying vibrational states,[38] and the sum of the three curves of Fig. 1(a), which incorporate appropriate line-strength factors,[56] provides a vertical-electronic approximation to the vibrationally averaged result that can be compared directly with corresponding cross-sectional measurements.[25-28] In Fig. 1(b) are shown the partial-channel IVO photoionization cross section for production of $X^2\Pi_g O_2^+$ parent ions and corresponding results obtained from recent line-source[25] and (e, 2e) dipole oscillator-strength measurements.[28] Although there is considerable structure in the line-source measurements at lower energy, which is presumably due to the presence of autoionizing Rydberg series converging on higher ionic states and to vibrational structures,[40] and there is a small quantitative discrepancy at intermediate energy, it is quite clear that the experimental and theoretical values are in good agreement. The small quantitative discrepancy near the maximum at ~28 eV in Fig. 1(b) can perhaps be attributed to the relatively small $9\delta_u$ basis employed (Table II), presumably making the description of the $1\pi_g \rightarrow k\delta_u 3d$ resonance feature in Fig. 1(a) somewhat imprecise. It is particularly satisfying that the calculations for this channel are in good agreement with experiment at higher energies, where the resonance feature does not contribute and a reliable description

of the scattering functions can be expected in the basis employed. The experimental data of Fig. 1(b) evidently provides substantial support for the presence of the $1\pi_g \rightarrow k\pi_u$-3d and $k\delta_u 3d$ resonances in the $(1\pi_g^{-1})X^2\Pi_g$ cross-section components of Fig. 1(a).

B. $1\pi_u$ spectra (I.P.=16.1eV)

The calculated $1\pi_u$ excitation series are compared with available spectral assignments and quantum-defect estimates in Table IV. Referring to Table II, it is seen that $23\sigma_g$, $16\pi_g$, and $13\delta_g$ pseudospectra are employed in this case. The indicated adiabatic ionization potential refers to the $a^4\Pi_u$ ionic state, and consequently, the calculated excitation series are made to converge on this value [Eq. (6a)]. Moreover, the calculated strengths cited refer only to the $a^4\Pi_u$ contributions, which correspond to 2/3 of the entire transition array.[56] Corresponding experimentally assigned series converging on the $A^2\Pi_u$ ionic state are generally within ~ 0.5 eV of the values cited,[51] although the higher-lying series converging on the $2^2\Pi_u$ and $3^2\Pi_u O_2^+$ states have apparently not been studied. The $2^2\Pi_u$ state in O_2^+ is reported at ~24eV, and the unassigned band at ~33eV in the photoelectron spectra is attributed here to the $3^2\Pi_u$ state.[28] As indicated in the preceding section, the static-exchange approach employed here predicts the appearance of four parent O_2^+ ionic state [$a^4\Pi_u$,$A^2\Pi_u$,$2^2\Pi_u$,$3^2\Pi_u$], and corresponding partial-channel photoionization cross sections, upon

removal of a $1\pi_u$ electron. Since the discrete states of Table IV lie above the 12.1 eV $1\pi_g$ ionization potential, they can autoionize into the underlying continua. Although autoionization linewidth calculations are not reported here, the calculated positions should be relatively insensitive to the appropriate interaction with the background continua.

The calculated $1\pi_u \rightarrow n\sigma_g$ series is evidently in general agreement with the assigned $ns\sigma_g$ series leading to the $a^4\Pi_u$ ionic state, and when shifted by ~ 0.5eV with the corresponding series at slightly higher energy converging on the $A^2\Pi_u$ ionic state (not shown).[51] Moreover, both IVO and experimental values are in general agreement with the positons obtained from the Rydberg formula and appropriate quantum defects, also listed in the table. The n=3 resonance in the series is evidently $3s\sigma_g$ Rydberg in character ($n^* \sim 2$, $\delta \sim 1$), and there is no evidence of substantial valence-orbital contribution to this particular subchannel, since the corresponding photoionization profile [Fig. 2(a)] is monotonically decreasing. These results are in general accord with expectations and with previously reported studies of the $1\pi_u \rightarrow n\sigma_g/k\sigma_g$ and $1\pi \rightarrow n\sigma/k\sigma$ cross sections in N_2 and CO, respectively.[2,3]

There is no evidence of a strong $1\pi_u \rightarrow 1\pi_g$ transition in the present calculations due to the orthogonality constraint imposed, as indicated above. Since this excitation corresponds to the familiar $X^3\Sigma_g^- \rightarrow B^3\Sigma_u^-$ Schumann-Runge

system,[52,53] it is not necessary to perform a separate investigation of its position and intensity here. The experimentally assigned first member of the $nd\pi_g$ series is in some accord with the present calculations, although the theoretical position is higher, perhaps as a consequence of the orthogonality constraint, and the predicted intensity is apparently weak. The IVO $1\pi_u \rightarrow n\pi_g$ calculations are in reasonable agreement with the positions obtained from the Rydberg formula and appropriate quantum defects,[51] also shown in the table. Referring to Fig. 2(a), the corresponding $1\pi_u \rightarrow k\pi_g$ photoionization cross section is quite weak, although there is evidence of a very broad resonance like feature at ~30eV. Apparently the $1\pi_u^{-1}$ effective potential supports only one valencelike π_g orbital, which appears in the discrete spectrum in this case (Schumann-Runge transition). The $1\pi_u \rightarrow k\pi_g$ cross section in O_2 of Fig. 2(a) is apparently dissimilar in appearance from the previously reported corresponding $1\pi_u \rightarrow k\pi_g$ and $1\pi \rightarrow k\pi$ cross sections in N_2 and CO, respectively, which exhibit large peaks just above threshold.[2,3] Reexamination of the previously reported static-exchange calculations of $1\pi_u$ and 1π excitation and ionization spectra in N_2 and CO, however, indicates that $1\pi_u \rightarrow k\pi_g$ and $1\pi \rightarrow k\pi$ photoionization cross sections similar to that of Fig. 2(a) are obtained when appropriate projection techniques are used to isolate the strong $\pi \rightarrow \pi^*$ transitions in each case.[57]

The experimentally assigned first member of the $^1\pi_u \rightarrow nd\delta_g$ series is in some accord with the present calculations, although the IVO resonance transition apparently contains only weak contributions from 3d orbitals, since n*=3.2 in this case. Indeed, much of the intensity in this IVO channel is concentrated in the strong resonance in the $1\pi_u \rightarrow k\delta_g$ photoionization cross section of Fig. 2(a) at ~ 22eV. This feature can be attributed to the presence of compact δ_g 3d molecular orbitals in final state symmetry, similar to the case of the $1\pi_g \rightarrow k\delta_u$ channel [Fig. 1(a)]. Moreover, the $1\pi_u \rightarrow k\delta_g$ profile of Fig. 2(a) is highly similar to the previously reported corresponding $1\pi_u \rightarrow k\delta_g$ and $1\pi \rightarrow k\delta$ photoionization cross sections in N_2 and CO respectively.[2,3] As in these latter cases, diabatic calculations on the $(1\pi_u^{-1}\delta_g 3d)\,^3\Pi_u$ state in O_2 would be helpful in clarifying the nature of the resonancelike feature in this channel.

The $a^4\Pi_u$ and $A^2\Pi_u O$ ionic state potential curves are not as deep as is that of the $X^2\Pi_g$ ionic state, and their minima are shifted to somewhat larger internuclear separations ($R_e \sim 2.8a_0$).[40] Moreover, the $2^2\Pi_u$ and $3^2\Pi_u$ state curves are most likely repulsive.[40] Nevertheless, the Franck-Condon regions are still expected to be relatively limited in these cases,[38] and the sum of the three vertical photoionization curves of Fig. 2(a) should provide a virbrationally averaged cross section suitable for comparison with appropriately interpreted measured data. In Fig. 2(b)

the theoretically determined vertical electronic cross section so obtained for formation of $a^4\Pi_u$, $A^2\Pi_u$, $2^2\Pi_u$, and $3^2\Pi_u$ parent O_2^+ ionic states is compared with the results of recent line-source[25] and (e, 2e)[28] dipole oscillator-strength measurements. The $a^4\Pi_u$ and $A^2\Pi_u$ contributions are obtained from the (e, 2e) partial-channel data by subtracting the $b^4\Sigma_g^-$ channel contribution from the measured values corresponding to the sum of the $a^4\Pi_u$, $A^2\Pi_u$, and $b^4\Sigma_g^-$ channels.[28] Since the $b^4\Sigma_g^-$ cross section is not resolved by the (e, 2e) measurements, an approximation to its contribution is obtained using twice the measured $B^2\Sigma_g^-$ cross section (which is experimentally resolved),[28] employing the theoretically predicted ratio $b^4\Sigma_g^-/B^2\Sigma_g^- = 2$.[56] Support for this theoretically determined ratio is provided by the line-source branching-ratio measurements of the $b^4\Sigma_g^-$ and $B^2\Sigma_g^-$ contributions,[25] which are precisely in the ratio 2:1 at the highest energy reported. To the sum of $a^4\Pi_u$ and $A^2\Pi_u$ partial-channel cross sections are added the $2^2\Pi_u$ contribution and the separately resolved contribution appearing at 33 eV in the photoelectron spectra,[28] which is here assigned as the $3^2\Pi_u O_2^+$ parent ionic state. The $2^2\Pi_u$ cross section is separated from the $c^4\Sigma_u^-$ channel with which it is degenerate by making use of the corresponding line-source data,[25] which indicates the former contributes ~ 70% to the combined $2^2\Pi_u$ and $c^4\Sigma_u^-$ bands. In adding the $2^2\Pi_u$ and $3^2\Pi_u$ contributions to the $a^4\Pi_u$ and $A^2\Pi_u$ cross sections it is, of course, necessary to refer the former to the $a^4\Pi_u$ threshold at ~ 16 eV. Although this procedure perhaps takes

some liberties with the experimental data, it is seen from Fig. 2(b) that generally good agreement between theory and experiment is obtained. The structure in the measurements at lower energy is presumably a consequence of autoionizing states and vibrational features. Since the calculated $1\pi_u \rightarrow k\delta_g 3d$ resonance appears in this spectral region, the measurements do not provide an unambiguous experimental verification in this case, although the experimental results are compatible with its presence. Moreover, the $2^2\Pi_u$ and $3^2\Pi_u$ partial-channel cross sections separately have maxima ~ 5 eV above their thresholds, in general support of the $1\pi_u \rightarrow k\delta_g 3d$ feature of Fig. 2(a).

C. $3\sigma_g$ spectra (I.P. = 18.2 eV)

The calculated $3\sigma_g$ excitation series and ionization cross sections are shown in Table V and Fig. 3, respectively. Table II indicates that $23\sigma_u$, $16\pi_u$, and $9\delta_u$ pseudospectra are employed in calculating the $3\sigma_g$ excitation and ionization cross sections. The calculated energies are made to converge on the experimentally observed $b^4\Sigma_g^- O_2^+$ state, and the strengths shown correspond to contributions from series converging on this state only, which accounts for $\frac{2}{3}$ of the entire transition array.[56] Evidently the $3\sigma_g \rightarrow n\sigma_u$ IVO series is in very good agreement with the assigned $np\sigma_u$ series,[51,58] and with estimates obtained from quantum defects. Of course, the ef-

fects of autoionization must be included in order to obtain a quantitative comparison of intensities. The n = 3 resonance transition in the series is essentially Rydberg ($n^* \sim 2.2$, $\delta \sim 0.8$) in character, and there is no evidence of a strong $3\sigma_g \rightarrow \sigma_u 2p$ intravalence excitation present in the discrete spectrum. However, referring to Fig. 3(a), the $3\sigma_g \rightarrow k\sigma_u$ IVO photoionization channel has a prominent resonancelike feature at ~20 eV, which can be attributed to the presence of valencelike $\sigma_u 2p$ orbitals in the $k\sigma_u$ photoionization continuum. Similar resonances appear in the $k\sigma_u$ and $k\sigma$ continua of N_2 and CO, respectively,[1-3] and presumably related valencelike diabatic $2^3\Sigma_u^-$, $3^3\Sigma_u^-$ states corresponding to $b^4\Sigma_g^-$ and $B^2\Sigma_g^-$ parentages, respectively, are obtained at 18.4 and 20.9 eV from recent CI calculations.[55]

The calculated $3\sigma_g \rightarrow n\pi_u$ excitations are evidently in very good agreement with the experimental positions and quantum defect estimated for the $np\pi_u$ series, although the strong intensity assignment is clearly at variance with the theoretical results. Evidently, the corresponding $3\sigma_g \rightarrow k\pi_u$ photoionization cross section [Fig. 3(a)] is very weak, although there is some evidence of a broad high-energy maximum at ~30 to 40 eV, presumably corresponding to the associated resonance at ~30 eV in the $1\pi_g \rightarrow k\pi_u$ cross section [Fig. 1(a)].

The Franck-Condon factors for production of $b^4\Sigma_g^-$ and $B^2\Sigma_g^-$ ionic states evidently favor a narrow (~ 0.5 eV) band of low-lying vibrational states, and do not extend into the dissociative photoionization continuum.[38,40] Consequently, the

two subchannel components for vertical photoionization of Fig. 3(a) are summed and compared in Fig. 3(b) with the results of recent line-source[25] and (e, 2e)[28] dipole oscillator-strength measurement. The (e, 2e) results shown are simply three times the measured $B^2\Sigma_g^-$ channel cross section, making use of the theoretically predicted ratio $b^4\Sigma_g^-/B^2\Sigma_g^- = 2$ indicated previously.[56] Although the theoretical and experimental results are evidently in general agreement, it is not entirely clear if the predicted $3\sigma_g \rightarrow k\sigma_u$ resonance feature is experimentally verified, since it appears near threshold in the region of possible vibrational and autoionizing structure. Nevertheless, the presence of a resonance-like feature just above threshold in the $3\sigma_g \rightarrow k\sigma_u$ cross section is consistent with the experimental data of Fig. 3(b), with the absence of a strong intravalence transition in the corresponding discrete spectrum (Table V), with the appearance of a similar weak resonancelike feature in the $1\pi_g \rightarrow k\sigma_u$ cross section of Fig. 1(a), and with the recent valence-basis calculations for the $2^3\Sigma_u^-$ and $3^3\Sigma_u^-$ diabatic states.[55] Moreover, it is of considerable interest to note that measurements of the K-edge photoabsorption cross section in O_2 indicate the presence of a resonancelike feature at or just above the photoionization threshold.[22-24] This feature presumably can be assigned to the $1\sigma_g \rightarrow k\sigma_u$ channel, and corresponds to the related $3\sigma_g \rightarrow k\sigma_u$ resonance of Fig. 3(a), providing further indirect support for the presence of a valencelike $\sigma_u 2p$ contribution to the $k\sigma_u$ continuum in O_2.

D. Valence-shell photoabsorption cross section

A further comparison between theory and experiment is provided by the results of recent synchrotron radiation,[26] and electron-impact and (e, e + ion) coincidence studies[28] of total absorption and O_2^+ and O^+ photoproduction in O_2 in the 18 to 70 eV energy interval. In order to obtain a meaningful comparison between theory and experiment in this case it is necessary to refer the $2^2\Pi_u$ and $3^2\Pi_u$ partial-channel contributions to the appropriate thresholds (24 and 33 eV, respectively), rather than to the $a^4\Pi_u$ threshold, as in Fig. 2(b). When this procedure is followed, the $1\pi_u^{-1}$ contribution will exhibit three distinct thresholds, associated with the $a^4\Pi_u$ and $A^2\Pi_u$, $2^2\Pi_u$, and $3^2\Pi_u$ states, respectively. In the absence of appropriate line shape calculations, the contributions to the total cross section from autoionizing states converging on the $2^3\Pi_u$ and $3^2\Pi_u$ thresholds are neglected, resulting in small discontinuities in these cases. Alternatively, if the states below these two thresholds are included in the S-T procedure, corresponding to introduction of very broad autoionization widths, the discontinuities are no longer present and the cross section increases somewhat in these regions. Finally, the relative contributions of the $A^2\Pi_u$, $2^2\Pi_u$, and $3^2\Pi_u$ partial-channel cross sections are obtained from a simple three-term O_2^+ configuration-interaction calculation in which the experimentally observed thresholds are introduced as constraints. The results of this semiempirical analysis, which is in the spirit of the use of experi-

mental ionization thresholds in Eqs. (6), indicate that the $A^2\Pi_u$ cross section is very weak, whereas the $2^2\Pi_u$ and $3^2\Pi_u$ contributions are in the ratio ~2:1. These predictions are in accord with the measured (e, 2e)$2^2\Pi_u$ and $3^2\Pi_u$ cross sections,[28] and with the apparent weak contribution the $A^2\Pi_u$ state makes to the high-resolution photoelectron spectra.[38] although not with previously reported theoretical studies.[59]

In Fig. 4 the results of the present IVO calculations for photoionization of the $1\pi_g$, $1\pi_u$, and $3\sigma_g$ orbitals in O_2 constructed as indicated above, are compared with measured cross sectional values. Evidently, the theoretical results are in good agreement with the measured photoabsorption cross section at energies $\lesssim$ 30 eV, whereas the measured photoabsorption cross section is greater than the theoretical result above ~30 eV, presumably as a consequence of dissociative ($2\sigma_g$, $2\sigma_u$) and two-electron photoionization. Moreover, the inflection in the data at ~40 eV can be attributed to an increase in O^+ production at this energy.[28] At higher energies the calculations approach the measured photoionization cross section for O_2^+ production, and consequently are in accord with expectations. Although the total cross sectional measurements do not provide direct evidence regarding resonance features, the presence of a maximum just above threshold in the measured values is not incompatible with the calculations, providing additional indirect support for the $3\sigma_g \rightarrow k\sigma_u$ resonance.

V. Resonance Features

The various resonance features appearing in the partial-channel photoabsorption cross sections in molecular oxygen warrant further summarizing discussion. Table VI provides a summary of the theoretical assignments and positions, and of the corresponding experimental estimates. The energies given in the first column are taken from recent valence-basis configuration-interaction calculations,[55] which refer to diabatic states, rather than spectroscopic states. Evidently, the predicted IVO and CI positions are in general agreement for the lowest-lying states of each symmetry. This suggests, as indicated above and discussed further below, that the positions of resonances in photoionization cross sections are determined in large measure by the diabatic approximation, although the shapes of the resonance cross sections are sensitive to the details of Rydberg-valence interaction in the continuum. Table VI emphasizes the very good agreement obtained between the separated-channel static-exchange results and the estimated positions of the measured photoionization resonances.

Although the results of Table VI are satisfactory, it is desirable to provide a somewhat more detailed characterization of the resonance features in the photoionization profiles in molecular oxygen. Referring to Fig. 1(a), the $1\pi_g \rightarrow k\pi_u$ and $1\pi_g \rightarrow k\delta_u$ resonances are attributed in the foregoing discussion (Sec. IV.A) to contributions to the photoionization continua from relatively compact pre-Rydberg

3d atomic oxygen orbitals (Table II). This view is in accord with the observation that 3d oxygen orbitals do not contribute significantly to the discrete $1\pi_g \rightarrow n\pi_u$ excitation series,[50] and with the evident highly similar natures of the $1\pi_g \rightarrow k\pi_u$ and $1\pi_g \rightarrow k\delta_u$ profiles. Nevertheless, it is only possible to make an unambiguous assignment in the case of the $1\pi_g \rightarrow k\delta_u$ profile, since the supplemental basis functions employed are all of d_{xy} type in this case (Table II). For the $1\pi_g \rightarrow k\pi_u$ profile it is possible that the relatively compact portion of the oxygen and CM p_x basis (Table II) can contribute significantly to the resonance feature. Of course, the presence of a well-defined n = 3 member in the discrete $np\pi_u$ series (Table III) makes this possibility somewhat less likely. Configuration-interaction calculations that include the $(1\pi_g^{-1}\delta_u 3d)^3\Pi_u$ and $(1\pi_g^{-1}\pi_u 3d)^3\Sigma_u^-$ configurational states, which are apparently unavailable at present, would be helpful in this connection, as indicated above. Presumably the appropriate diabatic curves, which should correlate with the dipole allowed $(2p^{-1}3d)^3D^0$ atomic oxygen state in the separated-atom limit, cross the outer limbs of the Rydberg series converging on the $X^2\Pi_g$ ionic state (Table III), and become photoionization resonances at the ground-state equilibrium internuclear separation. By contrast, the $(1\pi_g^{-1}\pi_u 3p)^3\Sigma_u^-$ diabatic state presumably correlates with the $(2p^{-1}3p)^5P^e$ atomic oxygen state in the separated-atom limit, and, consequently, is not dipole connected to the ground state in this limit. It is not possible to provide an unambiguous molecu-

lar-orbital characterization of the small but distinct feature near threshold in the $1\pi_g \rightarrow k\sigma_u$ channel [Fig. 1(a)] on the basis of the present calculations. However the absence of a strong valencelike member in the calculated and observed $np\sigma_u$ excitation series (Table III), as well as the results of previously reported CI calculations,[54,55] which indicate the presence of a diabatic valence state crossing the Rydberg series, suggests that this small feature can be attributed to a compact $\sigma_u 2p$ orbital lying just above the threshold. Indeed, referring to Table VI, the position of the diabatic $(1\pi_g^{-1}\sigma_u 2p)^3\Pi_u$ state is seen to be in rather good agreement with the present IVO result. Since only the $X^2\Pi_g O_2^+$ ionic state is produced upon removal of a $1\pi_g$ electron, the calculated orbital photoionization cross sections [Fig. 1(a)] are simply related to the experimental results [Fig. 1(b)], which later provide considerable support for the existence of the predicted $\pi_u 3d$ and $\delta_u 3d$ resonance features.

Referring now to the $1\pi_u$ photoionization profiles of Fig. 2(a), the prominent feature in the $1\pi_u \rightarrow k\delta_g$ subchannel can be attributed to contributions from relatively compact pre-Rydberg 3d atomic oxygen orbitals (Table II), in accordance with the observation that the discrete resonance in the $nd\delta_g$ series (Table IV) has an effective principal quantum number of ~ 3.2. Evidently, the opening of the $1\pi_u$ shell provides a somewhat more attractive potential for the $k\delta_g$ spectrum than does the $1\pi_g$ shell for the $k\delta_u$ spectrum, since the resonance in the former appears at significantly lower

energy (~5 eV above threshold) than does the latter (~16 eV above threshold). Recall that a prominent $1\pi_u \rightarrow k\delta_g$ resonance feature also appears in the previously reported corresponding cross section in N_2.[2] The appropriate diabatic state calculations for these configurations in O_2 and N_2 have, unfortunately, not been reported. Nevertheless, it can be expected that the $(1\pi_u^{-1}\delta_g 3d)^3\Pi_u$ diabatic state, which should correlate with the dipole allowed $(2p^{-1}3d)^3D^0$ atomic oxygen state, crosses the outer limbs of the $nd\,\delta_g$ Rydberg series (Table IV) and becomes a photoionization resonance at the ground-state equilibrium internuclear separation. The $1\pi_u \rightarrow k\sigma_g$ profile is evidently monotonic, and, of course, joins smoothly to the Stieltjes histogram in the discrete spectral interval,[35] which is dominated by the strong $1\pi_u \rightarrow 3s\,\sigma_g$ Rydberg transition (Table IV). Again, a similar behavior is seen in the corresponding profile in N_2.[2] By contrast, the $1\pi_u \rightarrow k\pi_g$ profile in N_2 shows a strong peak near threshold, whereas the present $1\pi_u \rightarrow k\pi_g$ cross section in O_2 [Fig. 2(a)] is flat and broad, with no evidence of a large contribution near threshold. As indicated above, re-examination of the N_2 calculations suggests that the large threshold value is a consequence of a $\pi \rightarrow \pi^*$ contribution. When appropriate projection procedures are employed in N_2 to localize the $\pi \rightarrow \pi^*$ contribution, a $1\pi_u \rightarrow k\pi_g$ photoionization profile similar to that of Fig. 2(a) is obtained.[57] Recall that the strong $1\pi_u \rightarrow 1\pi_g$ intravalence transition is not included in the present calculations, thereby eliminating its possible

contamination of the continuum. Because four parent O_2^+ ionic states [$a^4\Pi_u$, $A^2\Pi_u$, $2^2\Pi_u$, $3^2\Pi_u$] are formed upon removal of a $1\pi_u$ electron, comparison with experiment must be made with care. It is found that when the measured $a^2\Pi_u$ and $A^2\Pi_u$ contributions, which are not separately resolved, are combined with the measured $2^2\Pi_u$ and $3^2\Pi_u$ contributions, the latter being shifted to the $a^4\Pi_u$ threshold, the theoretical and experimental results are in good agreement . Moreover, the three separately measured cross sections [$a^4\Pi_u + A^2\Pi_u$, $2^2\Pi_u$, $3^2\Pi_u$] exhibit peaks ~5 eV above their respective thresholds, providing substantial support for the presence of the predicted $1\pi_u \rightarrow k\delta_g 3d$ resonance feature.

The appearance of a prominent resonancelike $\sigma_u 2p$ feature in the $3\sigma_g \rightarrow k\sigma_u$ cross section of Fig. 3(a) is in complete accord with the results of the previous investigations in N_2 and CO,[1-3] with the foregoing remarks made in connection with the $1\pi_g \rightarrow k\sigma_u$ channel, and with the observation that the discrete $3\sigma_g \rightarrow n\sigma_u$ series (Table V) does not include an intravalence contribution. Moreover, the valence-basis CI calculations (Table VI) predict the presence of two diabatic states, corresponding to $b^4\Sigma_g^-$ and $B^2\Sigma_g^-$ parentages, at the appropriate resonance position. Finally, the presence of a prominent feature in the O_2K-edge cross section just above threshold, which can be given a $1\sigma_g \rightarrow k\sigma_u$ assignment, provides additional support for the appearance of a $\sigma_u 2p$ contribution in the photoionization continuum.[24]

Although the experimentally determined partial-channel

cross sections for $1\pi_g$, $1\pi_u$, and $3\sigma_g$ photoionization in O_2 do not provide unambiguous verification of the calculated resonance features, the measured values are certainly compatible with the theoretical results and with the corresponding interpretations. Moreover, the independent measurements of the total photoabsorption and ionization cross sections shown in Fig. 4 are also compatible with the present calculations, and perhaps also provide some support for the $3\sigma_g \rightarrow k\sigma_u 2p$ resonancelike feature slightly above the corresponding threshold.[60]

VI. CONCLUDING REMARKS

The qualitative discussions of electronic excitation and ionization processes presented here, and the quantitative separated-channel, static-exchange calculations upon which they are based, attempt to provide an overall elementary account of both the discrete and continuous portions of the valence spectrum in molecular oxygen. Use of the Stieltjes-Tchebycheff technique and L^2 calculations allows rather straightforward application of familiar molecular-orbital concepts to the photoionization continua corresponding to various occupied orbitals, and thereby provides a basis for discussing the discrete and continuous excitations from a common perspective. Most important, the concepts of intense intravalencelike transitions on the one hand, and generally weaker Rydberg-like transitions on the other, are seen to carry over in a natural way into the photoionization continua.

In particular, the $1\pi_g$ photoionization continuum in oxygen is seen to be dominated by features that are conveniently regarded as arising from the presence of $\pi_u 3d$, $\delta_u 3d$, and $\sigma_u 2p$ final-state resonancelike orbitals in the $k\pi_u$, $k\delta_u$, and $k\sigma_u$ channels, respectively, Similarly, the $1\pi_u$ and $3\sigma_g$ cross sections contain $\delta_g 3d$ and $\sigma_u 2p$ resonancelike features, respectively. These final-state valence orbitals do not contribute to the corresponding discrete spectral regions, but rather are associated with diabatic states that cross the outer limbs of the various Rydberg series as functions of internuclear distance, becoming photoionization resonance above the appropriate ionization potentials at the ground-state equilibrium separation.

In addition to providing an overall descriptive account of the electronic dipole excitation spectrum in molecular oxygen, the calculations reported here are seen to be in generally good quantitative accord with very recent corresponding experimental studies. Some care is required in making comparisons between theory and experiment in molecular oxygen, particularly since there are four final ionic states and corresponding cross sections associated with the removal of a $1\pi_u$ electron. Although the measured photoelectron spectra and partial-channel cross sections are relatively complex, good agreement between theory and experiment obtains when proper cognizance is taken of the ionic parentages of the various multiplet states. Although further computational refinements, including coupled-channel, static-exchange calculations, allowance for core polarization and

relaxation, explicit treatments of vibrational degrees of freedom, and of aspects of autoionizing states, will improve agreement with experiment, it is clear that the general approach employed here should continue to provide useful first approximations to discrete and continuous dipole excitation spectra in small molecules. Further computational applications are consequently in progress and will be reported subsequently.

ACKNOWLEDGEMENTS

The authors thank C. E. Brion and M. J. Van der Wiel for kindly making the results of their experimental studies available prior to publication, and for helpful correspondence. We also thank R. L. Blake for permission to cite his experimental results prior to publication, and A. U. Hazi for his help in clarifying the origins of the four $1\pi_u$ cross sections. Achknowledgement is made to the National Science Foundation for support provided to B.V.M., and to the Donors of the Petroleum Research Fund, administered by the American Chemical Society, and to the National Research Council, for providing support to P.W.L. The kind hospitality of J. O. Arnold and S. R. Langhoff of the NASA-Ames Research Center Computational Chemistry Group, and of D. Bershader of the Department of Aeronautics and Astronautics, Stanford University, to P.W.L. is also gratefully acknowledged.

REFERENCES AND NOTES

[1] T. N. Rescigno and P. W. Langhoff, Chem. Phys. Lett. 51, 65 (1977).

[2] T. N. Rescigno, C. F. Bender, B. V. McKoy, and P. W. Langhoff, J. Chem. Phys. 68, 970 (1978).

[3] N. Padial, G. Csanak, B. V. McKoy, and P. W. Langhoff, J. Chem. Phys. 69, 2992 (1978).

[4] P. W. Langhoff, S. R. Langhoff, and C. T. Corcoran, J. Chem Phys. 67, 1722 (1977).

[5] P. W. Langhoff, A. E. Orel, T. N. Rescigno, and B. V. McKoy, J. Chem. Phys. 69, 4689 (1978).

[6] Geoffry R. J. Williams and P. W. Langhoff, Chem. Phys. Lett. 60, 201 (1978).

[7] J. A. Samson and J. L. Gardner, J. Electron Spectrosc. Relat. Phenom. 8, 35 (1976).

[8] A. Hamnett, W. Stoll, and C. E. Brion, J. Electron Spectrosc. Relat. Phenom. 8, 367 (1976).

[9] G. R. Wight, M. J. Van der Wiel, and C. E. Brion, J. Phys. B 9, 675 (1976).

[10] E. W. Plummer, T. Gustafsson, W. Gudat, and D. E. Eastman, Phys. Rev. A 15, 2339 (1977).

[11] J. A. R. Samson, G. N. Haddad, and J. L. Gardner, J. Phys. B 10, 1749 (1977).

[12]R. B. Kay, Ph. E. Van der Leeuw, and M. J. Van der Wiel, J. Phys. B 10, 2513, 2521 (1977).

[13]P. R. Woodruff and G. V. Marr, J. Phys. B 9, L377 (1976); Proc. R. Soc. London Ser. A 358, 87 (1977).

[14]G. V. Marr, J. M. Morton, R. M. Holmes, and D. G. Mc Coy, J. Phys. B (to be published).

[15]J. L.Dehmer and D. Dill, Phys. Rev. Lett. 35, 213 (1975); J. Chem. Phys. 65, 5327 (1976).

[16]J. W. Davenport, Phys. Rev. Lett. 36, 945 (1976); Int. J. Quantum Chem. Symp. 11, 89 (1977).

[17]J. -T. J. Huang, F. O. Ellison, and J. W. Rabalais, J. Electron Spectrosc. Relat. Phenom. 3, 339 (1974).

[18]H. C. Tuckwell, J. Phys. B 3, 293 (1970).

[19]F. Hirota, J. Electron Spectrosc. Relat. Phenom. 9, 149 (1976).

[20]R. D. Hudson (Ed.) "Critical Review of Ultraviolet Photo-Absorption Cross Sections for Molecules of Astrophysical and Aeronomic Interest," Nat. Stand. Ref. Data Ser. Natl. Bur. Stand. 38 (1971).

[21]P. H. Krupenie, J. Phys. Chem. Ref. Data 1, 423 (1972).

[22]G. R. Wight and C. E. Brion, J. Electron Spectrosc. Relat. Phenom. 4, 313 (1974); A. P. Hitchcock and C. E. Brion, J. Phys. B. (to be published).

[23]R. E. LaVilla, J. Chem. Phys. 63, 2733 (1975).

[24]D. M. Barrus, R. L. Blake, A. J. Burek, K. C. Chambers, and A. L. Pregenzer, Phys. Rev. (to be published).

[25]J. A. R. Samson, J. L. Gardner, and G. N. Haddad, J. Electron Spectrosc. Relat. Phenom. 12, 281 (1977).

[26]G. Mehlman, D. L. Ederer, and E. B. Saloman, J. Chem. Phys. 68, 1862 (1978). See also L. C. Lee, R. W. Carlson, D. L. Judge, and M. Ogawa, J. Quant. Spectrosc. Radiat. Transfer 13, 1023 (1973).

[27]D. G. McCoy, J. M. Morton, and G. V. Marr, J. Phys. B (to be published).

[28]C. E. Brion, K. H. Tan, M. J. Van der Wiel, and Ph. E. Van der Leeuw, J. Electron Spectrosc. Relat. Phenom. 17, 101 (1979).

[29]P. W. Langhoff, C. T. Corcoran, J. S. Sims, F. Weinhold, and R. M. GLover, Phys. Rev. A 14, 1042 (1976).

[30]C. T. Corcoran and P. W. Langhoff, J. Math. Phys. 18, 651 (1977).

[31]P. W. Langhoff, Int. J. Quantum Chem. Symp. 8, 347 (1974); 11, 301 (1977).

[32]P. W. Langhoff, "The Stieltjes-Tchebycheff Approach to Molecular Photoionization Studies," in *Electron- and Photon-Molecule Collisions*, edited by T. N. Rescigno, B. V. McKoy, and B. Schneider (Plenum, New York, 1979), pp. 183-224.

[33]H. F. Schaefer III, *The Electronic Structure of Atoms and Molecules* (Addison-Wesley, Reading, MA, 1972); Ann. Rev. Phys. Chem. 27, 261 (1976).

[34]T. H. Dunning and P. J. Hay, in *Modern Theoretical Chemistry*, edited by H. F. Schaefer, III (Plenum, New York, 1976). Vol. 3, Chap. 1.

[35]P. W. Langhoff and C. T. Corcoran, J. Chem. Phys. 61, 146 (1974).

[36]D. W. Turner, C. Baker, A. D. Baker, and C. R. Brundle, *Molecular Photoelectron Spectroscoy* (Wiley, New York, 1970).

[37]K. Siegbahn, C. Nordling, G. Johansson, J. Hedman, P. F. Hedén, K. Hamrin, U. Gelius, T. Bergmark, L. O. Werme, R. Manne, and Y. Bauer, *ESCA Applied to Free Molecules* (North-Holland, Amsterdam, 1969).

[38]J. Raffery and W. G. Richards, Int. J. Mass Spectrom. Ion Phys. 6, 269 (1971); O. Edqvist, E. Lindholm, L. E. Selin, and L. Åsbrink, Phys. Scr. 1, 25 (1970).

[39]P. E. Cade and A. C. Wahl, At. Data Nucl. Data Tables 13, 339 (1974).

[40]F. R. Gilmore, J. Quant. Spectrosc. Radiat. Transfer. 5, 369 (1965).

[41]J. B. Rose and V. McKoy, J. Chem. Phys. 55, 5435 (1971).

[42]H. Lefebvre-Brion, C. Moser, and R. K. Nesbet, J. Mol. Spectrosc. 13, 418 (1964).

[43]E. U. Condon and G. H. Shortley, *The Theory of Atomic Spectra* (Cambridge U. P., London, 1963), p. 98.

[44]G. Herzberg, *Spectra of Diatomic Molecules* (Van Nostrand, New York, 1950), 2nd ed.

[45]K. Tanaka and M. Yoshimine, J. Chem. Phys. 70, 1626 (1979).

[46]R. S. Mulliken and C. A. Rieke, Rep. Prog. Phys. 8, 321 (1941).

[47]R. S. Mulliken and W. C. Ermler, *Diatomic Molecules* (Academic, New York, 1977).

[48]O. Sinanoglu, "Theory of Intravalency and Rydberg Transitions in Molecules," in *Chemical Spectroscopy and Photochemistry in the Vacuum Ultraviolet*, edited by C. Sandorfy, P. J. Ausloss, and M. B. Robin (Reidel, Boston, MA, 1974), pp. 337-384.

[49]Y. Tanaka and T. Takamine, Tokyo Inst. Phys. Chem. Res. 39, 437 (1942).

[50]D. C. Cartwright, W. J. Hunt, W. Williams, S. Trajmar, and W. A. Goddard, J. Chem. Phys. 8, 2436 (1973).

[51]E. Lindholm, Ark. Fys. 40, 117 (1969).

[52]K. Morokuma and H. Konishi, J. Chem. Phys. 55, 402 (1971).

[53]H. F. Schaefer, III and W. H. Miller, J. Chem. Phys. 55, 4107 (1971).

[54]R. J. Buenker and S. D. Peyerimhoff, Chem. Phys. 8, 324 (1975); Chem. Phys. Lett. 34, 225 (1975).

[55]R. P. Saxon and B. Liu, J. Chem. Phys. 67, 5432 (1977).

[56]P. W. Langhoff, A. Gerwer, C. Asaro, and B. V. McKoy, Int. J. Quantum Chem. Symp. (to be published).

[57]T. N. Rescigno, A. Gerwer, B. V. McKoy, and P. W. Langhoff, Chem. Phys. Lett. 66, 116 (1979).

[58]J. Leclercq, Ann. Astrophys. 30, 93 (1967).

[59]D. N. Dixon and S. E. Hull, Chem. Phys. Lett. 3, 367 (1969).

[60]T. Gustafsson (private communication) has recently completed high-resolution PES and partial-channel photoionization cross section studies in O_2 the results of which are in excellent accord with the present calculations, and which, in particular, verify the existence of the $3\sigma_g \rightarrow k\sigma_u \Sigma p$ resonance just above threshold. We thank Dr. Gustafsson for making his results available prior to publication.

TABLE I. Static-exchange open-shell potentials in molecular oxygen.[a,b]

Γ^i	$3\sigma_g$	$1\pi_u^x$	$1\pi_u^y$	$1\pi_g^x$	$1\pi_g^y$
$3\sigma_g \rightarrow k\sigma_u$	$\frac{1}{2}/-1$	1/1	1/1	$\frac{1}{2}/\frac{1}{2}$	$\frac{1}{2}/\frac{1}{2}$
$\rightarrow k\pi_u^x$	$\frac{1}{2}/-1$	1/1	1/1	$\frac{1}{2}/\frac{1}{2}$	$\frac{1}{2}/\frac{1}{2}$
$1\pi_u^x \rightarrow k\sigma_g$	1/1	$\frac{3}{4}/\frac{1}{2}$	$\frac{3}{4}/\frac{1}{2}$	$\frac{1}{2}/\frac{1}{2}$	$\frac{1}{2}/\frac{1}{2}$
$\rightarrow k\pi_g^x$	1/1	$\frac{1}{2}/-3$	1/5	$\frac{1}{2}/\frac{1}{2}$	$\frac{1}{2}/\frac{1}{2}$
$\rightarrow k\delta_g^{xy}$	1/1	$\frac{3}{4}/\frac{1}{2}$	$\frac{3}{4}/\frac{1}{2}$	$\frac{1}{2}/\frac{1}{2}$	$\frac{1}{2}/\frac{1}{2}$
$1\pi_g^x \rightarrow k\sigma_u$	1/1	1/1	1/1	$\frac{1}{4}/\frac{1}{2}$	$\frac{1}{4}/\frac{1}{2}$
$\rightarrow k\pi_u^x$	1/1	1/1	1/1	$-\frac{1}{4}/-1$	$\frac{3}{4}/3$
$\rightarrow k\delta_u^{xy}$	1/1	1/1	1/1	$-\frac{1}{4}/-1$	$\frac{3}{4}/3$

TABLE I. - FOOTNOTES

[a]Values of the coefficients a_i^Γ/b_i^Γ appearing in the potential of Eq. (5), determined employing the procedures of J. B. Rose and V. McKoy, J. Chem. Phys. 55, 5435 (1971).

[b]The $1\sigma_g$, $1\sigma_u$ and $2\sigma_g$, $2\sigma_u$ orbitals remain doubly occupied and, consequently, $a_i^\Gamma = 1$, $b_i^\Gamma = 1$ in these cases.

TABLE II. Supplemental Gaussian basis for molecular oxygen calculations.[a]

Location	Type	Number	Exponent range[b]
		(σ_g/σ_u) symmetry	
0/0	s/s	4/4	2.0-0.12/0.0862-0.0024
0/0	p_z/p_z	4/4	2.0-0.12/0.0637-0.00169
c.m./c.m.	s/p_z	12/12	0.2-0.00052/0.2-0.00052
		(π_g/π_u) symmetry	
0/0	p_x/p_x	4/4	0.7-0.6/0.7-0.06
0/0	d_{xz}/d_{xz}	4/4	0.7-0.1/0.7-0.06
c.m./c.m.	d_{xz}/p_x	6/6	0.5-0.025/0.025-0.001
		(δ_g/δ_u) symmetry	
0/0	d_{xy}/d_{xy}	5/9	0.5-0.1/0.5-0.005
c.m./c.m.	$d_{xy}/...$	8/...	0.2-0.007/...

TABLE II. - FOOTNOTES

[a]Supplemental basis functions employed, in addition to the (10s, 5p, 1d)/[3s, 2p, 1d] valence basis, in solution of Eq. (3).

[b]Ratios of successive exponents vary geometrically.

TABLE III. $1\pi_g$ excitation spectra in O_2 (I.P. = 12.1 eV).

Present results[a] Energy (eV)/f Number	Experimental values[b] Energy (eV)/Intensity	Previous calculations[c] Energy (eV)/f Number
	$(1\pi_g)^3\Sigma_g^- \rightarrow (np\pi_u)^3\Sigma_u^-$	
9.42/0.00271	9.31/weak	9.44/0.00215
10.82/0.00076	10.46	10.85/0.00073
11.34/0.00032	11.36	11.32/0.00033
11.59/0.00016	11.54	...
11.76/...	11.62	...
	$(1\pi_g)^3\Sigma_g^- \rightarrow (np\sigma_u)^3\Pi_u$	
8.53/0.00000	...	7.99/...
10.16/0.00835	9.97/strong	9.98/0.00833
11.00/0.00549	10.98	10.96/0.00376
11.41/0.00285	11.36	11.32/0.00201
11.63/0.00160	11.54	...
11.75/0.00099	11.62	...
11.86/...	...	...
	$(1\pi_g)^3\Sigma_g^- \rightarrow (n\delta_u)^3\Pi_u$	
11.22/0.00015	...	10.68/...
11.74/...	...	11.41

TABLE III. - FOOTNOTES

[a]Values obtained from Eqs. (3) to (6) and appropriate multiplet line-strength factors employing the basis sets described in Sec. III and Table II. The indicated series are made to converge on the experimentally determined $X^2\Pi_g$ ionic state, as discussed in the text.

[b]Spectral assignments and intensities taken from Y. Tanaka and T. Takamine, Tokyo Inst. Phys. Chem. Res. 39, 437 (1942); E. Lindholm, Ark. Fys. 40, 117 (1969). See also the tabulations of P. H. Krupenie, J. Phys. Chem. Ref. Data 1, 423 (1972), and references cited therein.

[c]Previously reported IVO calculations of D. C. Cartwright, W. J. Hunt, W. Williams, S. Trajmar, and W. A. Goddard, J. Chem. Phys. 8, 2436 (1973). Additional theoretical calculations are reported by J. LeClereq, Ann. Astrophys. 30, 93 (1967); T. Betts and V. McKoy, J. Chem. Phys. 54, 113 (1971); H. F. Schaefer and W. H. Miller, J. Chem. Phys. 55, 4107 (1971); K. Morokuma and H. Konishi, J. Chem. Phys. 55, 402 (1971); R. J. Buenker and S. D. Peyerimhoff, Chem. Phys. 8, 324 (1975); Chem. Phys. Lett. 34, 225 (1975); R. P. Saxon and B. Liu, J. Chem. Phys. 67, 5432 (1977). The values cited for the $1\pi_g \rightarrow n\delta_u$ series are obtained from the Rydberg formula for n = 3 and 4 employing a quantum defect of 0.1. Estimates for f numbers obtained from the Coulomb approximation Ref. 35).

TABLE IV. $1\pi_u^-$ excitation spectra in O_2 (I.P. = 16.1 eV)

Present results[a] Energy (eV)/f Number	Experimental assignments[b] Energy (eV)/Intensity	Quantum-defect estimates[c] Energy (eV)/ f number
	$(1\pi_u)^3\Sigma_g^- \rightarrow (ns\sigma_g)^3\Pi_u$	
12.59/0.0925	12.35/strong	12.70/0.1361
14.70/0.0314	14.53	14.59/0.0403
15.42/0.0141	15.23	15.25/0.0170
15.76/0.0074	...	15.56/0.0087
15.93/0.0044	...	15.71/0.0050
16.03/0.0040	...	15.82/0.0032
	$(1\pi_u)^3\Sigma_g^- \rightarrow (nd\pi_g)^3\Sigma_u^-$	
14.88/0.00097	14.48/medium	14.48/0.00279
15.94/...	...	15.21/0.00115
	$(1\pi_u)^3\Sigma_g^- \rightarrow (nd\delta_g)^3\Pi_u$	
14.80/0.0196	14.58/medium	14.48/0.0669
15.53/0.0165	...	15.21/0.0275

TABLE IV. - FOOTNOTES

[a]As in Table III. The calculated energies are made to converge on the $a^4\Pi_u O_2^+$ ionic state, and the strengths refer to contributions from the series converging on this state only, as is discussed further in the text.

[b]Values taken from the tabulations of E. Lindholm, Ark. Fys. 40, 117 (1969). The entries refer to Rydberg series converging on the $a^4\Pi_u$ parent O_2^+ ionic state. Additional series converging on the $A^2\Pi_u$ ionic state are also reported at energies generally within ~ 0.5 eV of the values cited, although the series converging on the higher-lying $2^2\Pi_u$ (24 eV) and $5^2\Pi_u$ (33 eV) ionic states also formed upon removal of a $1\pi_u$ electron are apparently not reported. As indicated in the text, the familiar $X^3\Sigma_g^- \rightarrow B^3\Sigma_u^-$ Schumann-Runge transition is not included in the present calculations.

[c]Values obtained from the Rydberg formula and the Coulomb limit (Ref. 35) for n = 3, 4, ... using quantum defects of 1.0 and 0.1 for the ns and nd series, respectively.

TABLE V. $3\sigma_g$ excitation spectra in O_2 (I.P. = 18.2 eV).

Present results[a] Energy (eV)/f Number	Experimental Assignments[b] Energy (eV)/Intensity	Quantum-defect estimates[c] Energy (eV)/f Number
	$(3\sigma_g)^3\Sigma_g^- \rightarrow (np\sigma_u)^3\Sigma_u^-$	
15.45/0.0825	15.28/medium	15.63/0.1038
16.91/0.0307	16.93	16.95/0.0352
17.45/0.0147	17.44	17.46/0.0159
17.71/0.0081	17.69	17.72/0.0085
17.85/0.0049	17.83	17.86/0.0051
17.96/...	17.91	17.94/0.0033
	$(3\sigma_g)^3\Sigma_g^- \rightarrow (np\pi_u)^3\Pi_u$	
15.61/0.00622	15.55/strong	15.63/0.00631
16.96/0.00206	16.93	16.95/0.00214
17.47/0.00092	17.45	17.46/0.00097
17.72/0.00049	...	17.72/0.00052
17.90/...	...	17.86/0.00031

TABLE V. - FOOTNOTES

[a]As in Table III. The calculated energies are made to converge on the $b^4\Sigma_g^-$ parent O_2^+ ionic state, and the strengths refer to contributions from series converging on this state only, as is discussed further in the text.

[b]Spectral assignments taken from tabulations of J. Leclercq, Ann. Astrophys. 30, 93 (1967). See also the references cited in Footnote b of Table III. The entries refer to Rydberg series converging on the parent O_2^+ ionic $b^4\Sigma_g^-$ state. Additional series converging on the $^2\Delta_g$ and $B^2\Sigma_g^-$ ionic states are also reported at energies generally with ~ 2 eV of the values cited.

[c]As in Table IV, employing $\delta = 0.7$ for np series.

TABLE VI. Photoionization resonance assignments in molecular oxygen.

Valence-basis CI calculations[a] State/Energy (eV)	Static-exchange calculations[b] Transition/Energy (eV)	Experiment[c] Energy (eV)
	$3\Sigma_u^-$ resonances	
$B^3\Sigma_u^-/9.03$	$1\pi_u \rightarrow 1\pi_g 2p/...$	~ 6
$2, 3^3\Sigma_u^-/18.4, 20.9$	$3\sigma_g \rightarrow k\sigma_u 2p/21$	~21
...	$1\pi_g \rightarrow k\pi_u 3d/28$	~26
	$^3\Pi_u$ resonances	
$1^3\Pi_u/10.5$	$1\pi_g \rightarrow k\sigma_u 2p/12$	...
...	$1\pi_u \rightarrow k\sigma_g 3d/22$	~20
...	$1\pi_g \rightarrow k\delta_u 3d/28$	~26

TABLE VI. - FOOTNOTES

[a]R. P. Saxon and B. Liu, J. Chem. Phys. 67, 5432 (1977). The indicated values refer to vertical excitation energies at $R = 2.3a_0$. See also R. J. Buenker and S. D. Peyerimhoff, Chem. Phys. 8, 324 (1975); Chem. Phys. Lett. 34, 225 (1975).

[b]Values obtained from Tables III to V and Figs. 1 to 4.

[c]Estimates obtained form the references cited and data appearing in Figs. 1 to 4.

FIGURE CAPTIONS

Fig. 1. (a) Vertical electronic S-T oscillator-strength densities obtained from Eqs. (6) and appropriate multiplet factors for $1\pi_g \rightarrow k\sigma_u$, $k\pi_u$, and $k\delta_u$ ionization in O_2. (b) Partial-channel photoionization cross section for production of $(1\pi_g^{-1})X^2\Pi_g O_2^+$ ions; (——) vertical electronic S-T cross section; ●, line-source measurements (Ref. 25); ▲, (e, 2e) coincidence measurements (Ref. 28). 1 Mb = 10^{-18} cm^2.

Fig. 2. (a) As in Fig. 1(a) for $1\pi_u \rightarrow k\sigma_g$, $k\pi_g$, and $k\delta_g$ photoionization. (b) As in Fig. 1(b) for the production of $a^4\Pi_u$, $A^2\Pi_u$, $2^2\Pi_u$, and $3^2\Pi_u O_2^+$ ions. The (e, 2e) results are constructed as discussed in the text.

Fig. 3. (a) As in Fig. 1(a) for $3\sigma_g \rightarrow k\sigma_u$ and $k\pi_u$ photoionization. (b) As in Fig. 1(b) for the production of $b^4\Sigma_g^-$ and $B^2\Sigma_g^- O_2^+$ ions. The (e, 2e) results are constructed as discussed in the text.

Fig. 4. Valence-shell photoabsorption and ionization cross sections in O_2. S-T results as indicated; Experimental results; ●, total absorption cross section from electron impact dipole oscillator-strength studies (Ref. 28); ▲ photoabsorption measurements of

Fig. 4 (cont.).

the total cross section (Refs. 25 and 26); ■, O_2^+ photoionization cross section from (e, e + ion) dipole oscillator-strength studies (Ref. 28). 1 Mb = 10^{-18} cm^2.

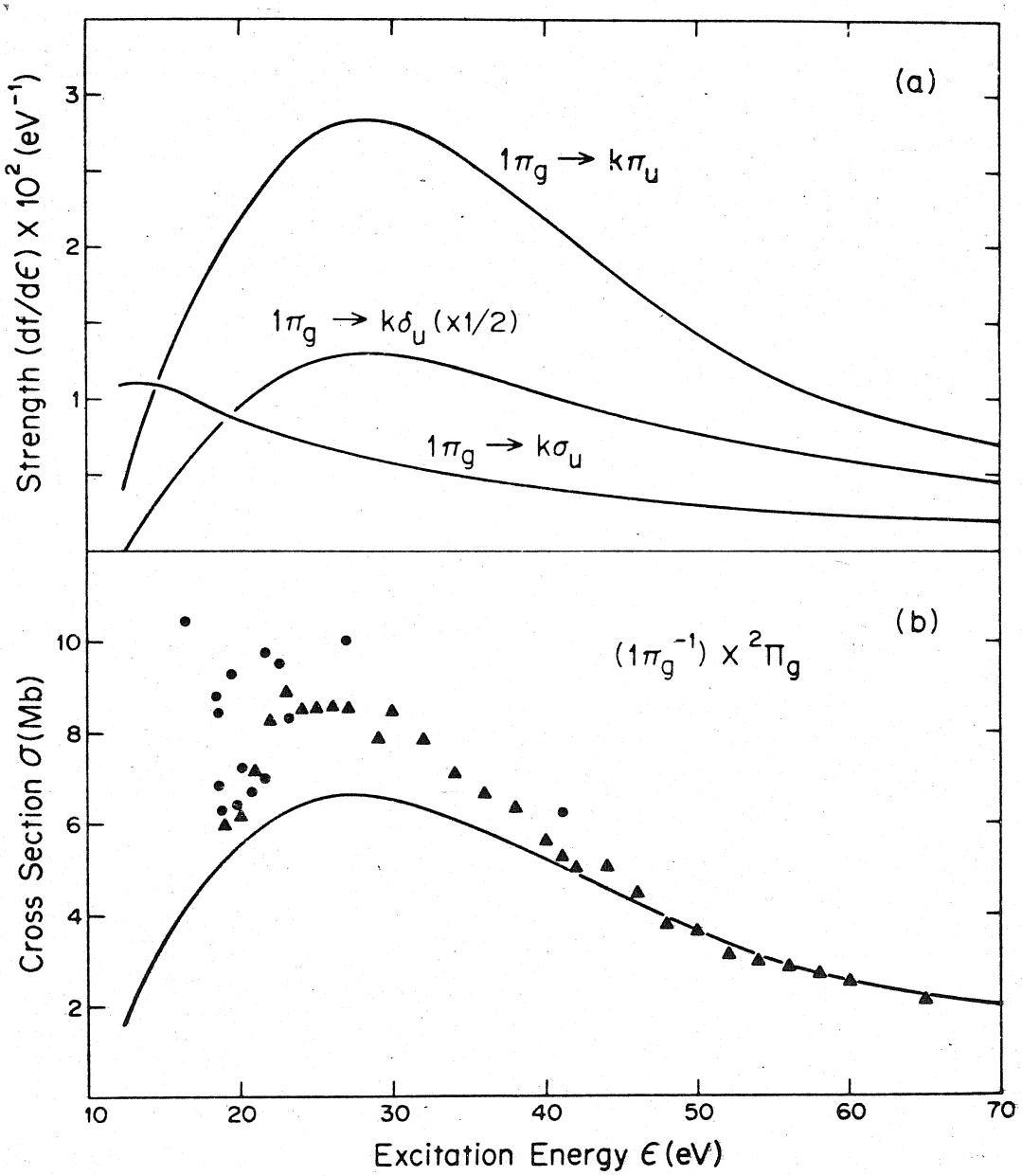
(a)
$1\pi_g \rightarrow k\pi_u$
$1\pi_g \rightarrow k\delta_u$ (x1/2)
$1\pi_g \rightarrow k\sigma_u$
Strength (df/dε) X 10^2 (eV^{-1})
(b)
$(1\pi_g^{-1}) \times {}^2\Pi_g$
Cross Section σ(Mb)
Excitation Energy ε (eV)

FIG.1

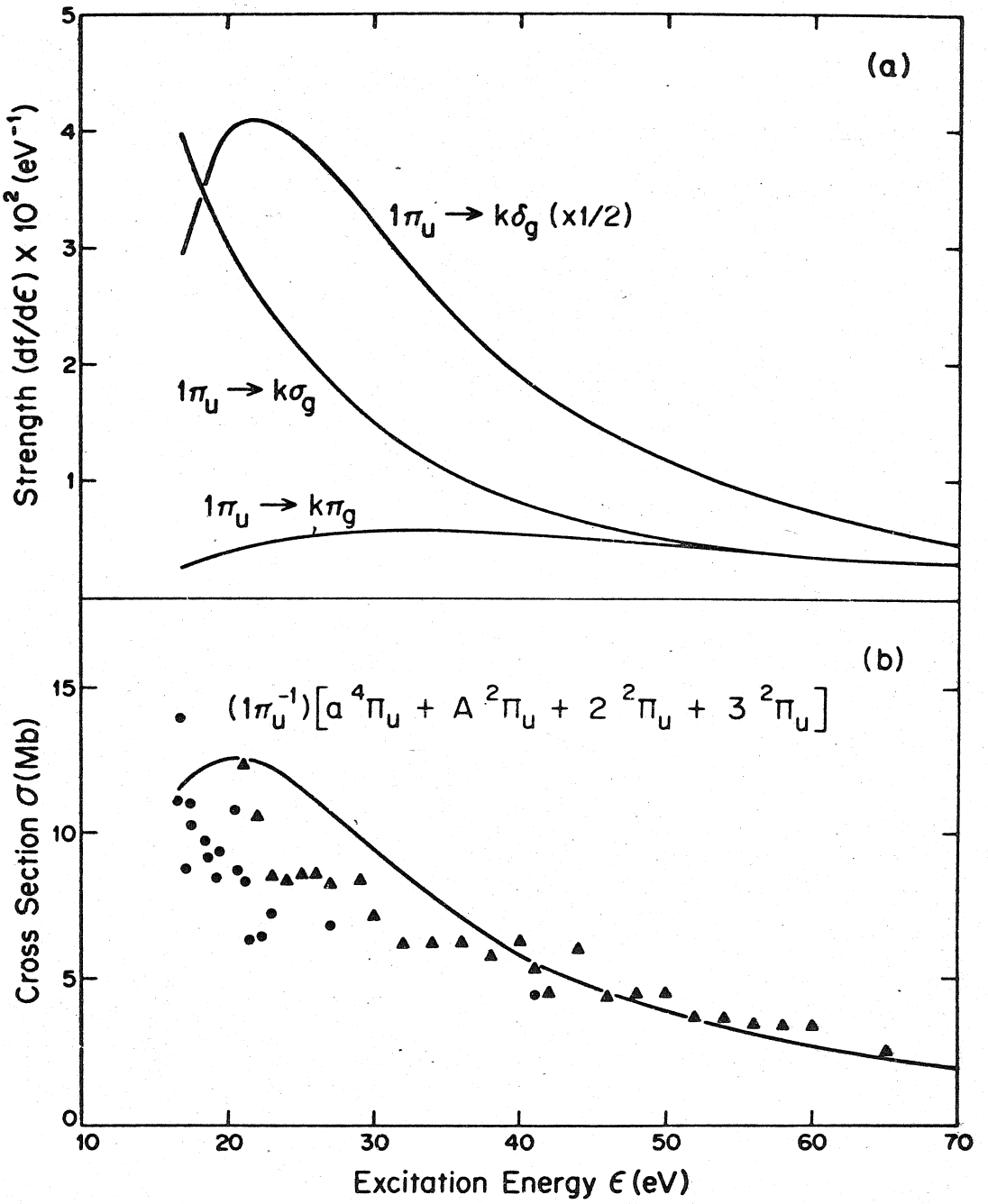
(a)
Strength (df/dε) X 10² (eV⁻¹)
1πu → kδg (x1/2)
1πu → kσg
1πu → kπg
(b)
Cross Section σ(Mb)
(1πu⁻¹)[a ⁴Πu + A ²Πu + 2 ²Πu + 3 ²Πu]
Excitation Energy ε (eV)

FIG. 2

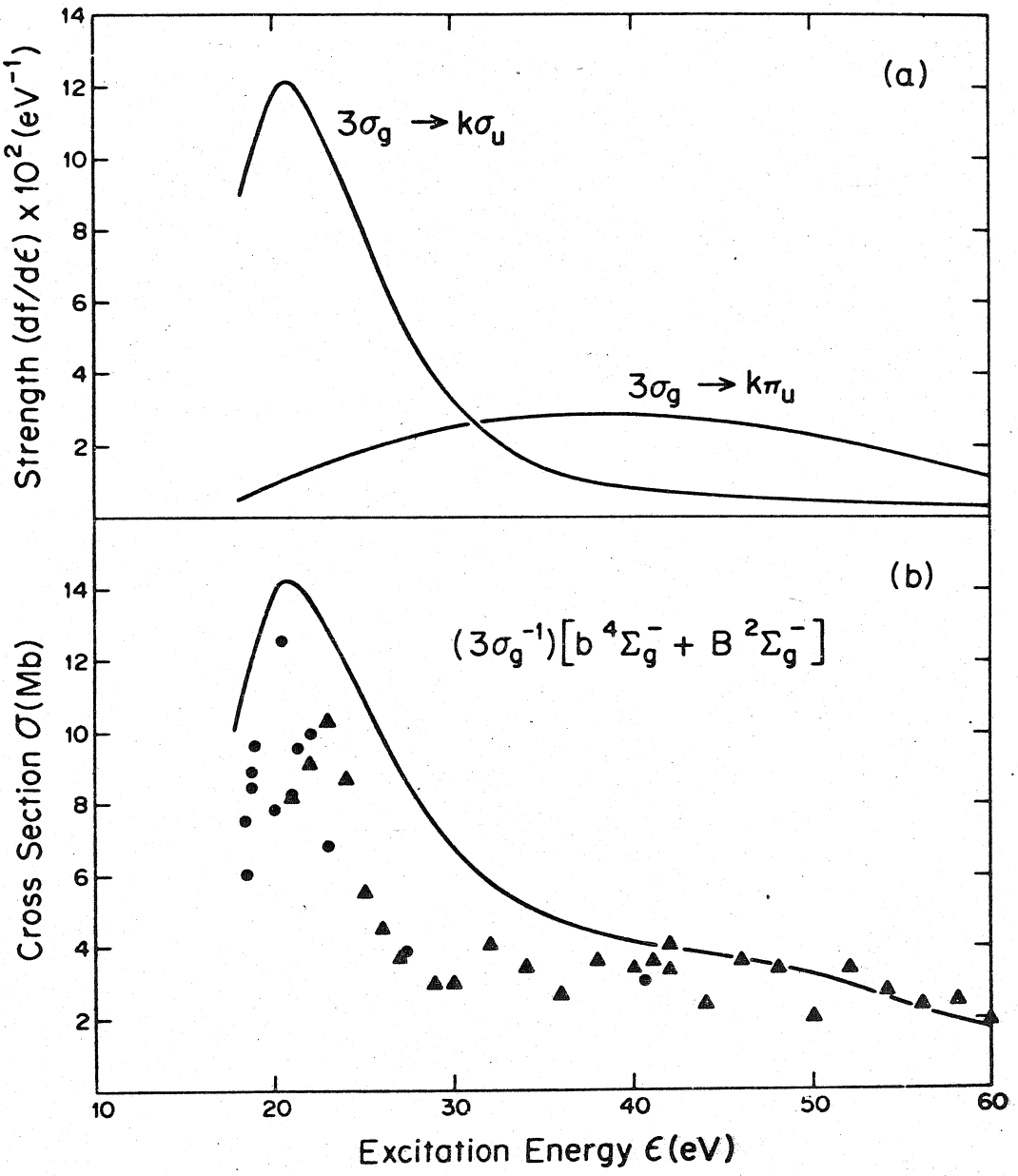
(a)
$3\sigma_g \rightarrow k\sigma_u$
$3\sigma_g \rightarrow k\pi_u$
Strength $(df/d\epsilon) \times 10^2 (eV^{-1})$
(b)
$(3\sigma_g^{-1})[b\,^4\Sigma_g^- + B\,^2\Sigma_g^-]$
Cross Section σ(Mb)
Excitation Energy ϵ(eV)

FIG.3

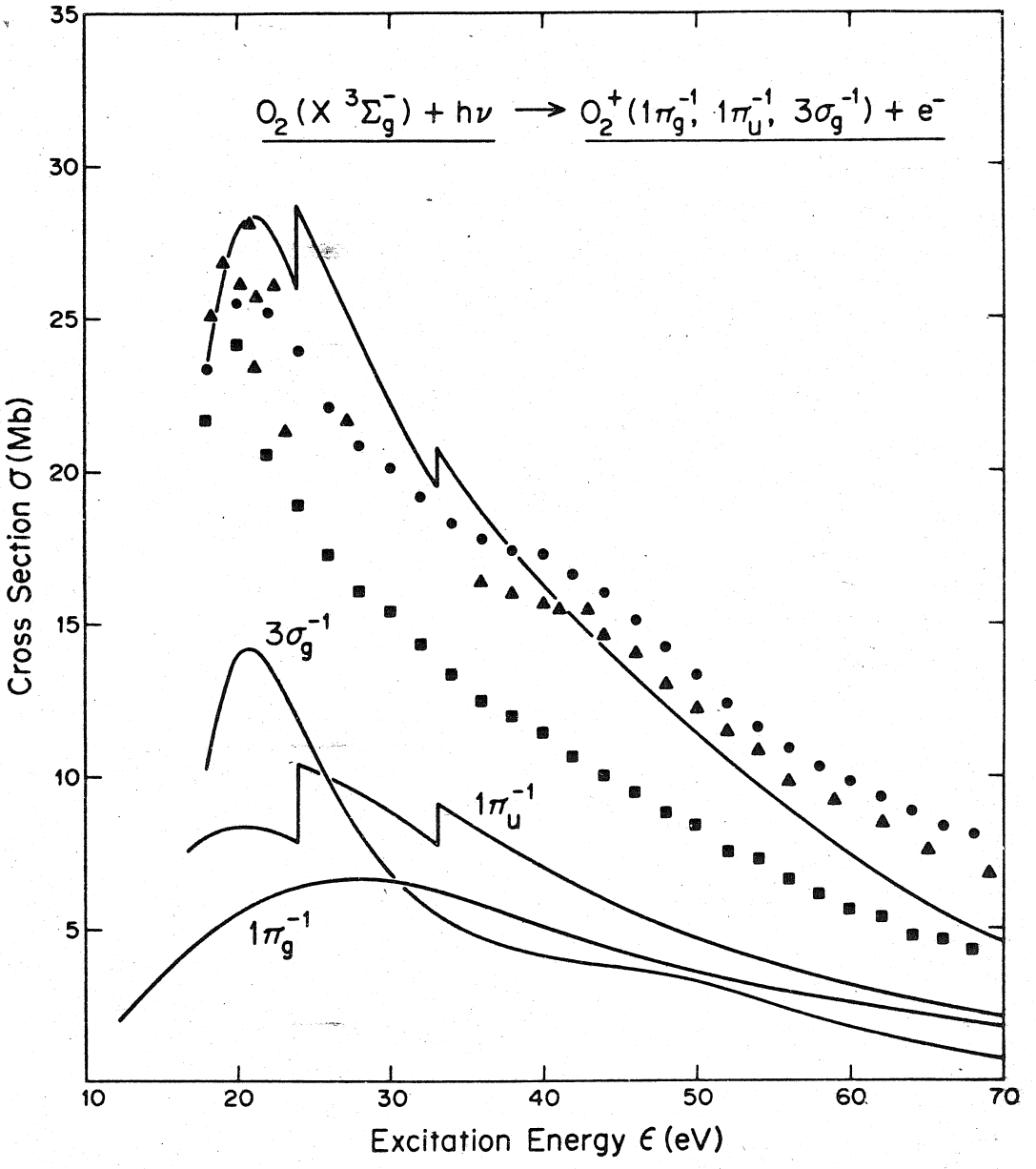
$O_2(X\ ^3\Sigma_g^-) + h\nu \longrightarrow O_2^+(1\pi_g^{-1}, 1\pi_u^{-1}, 3\sigma_g^{-1}) + e^-$
Cross Section σ (Mb)
Excitation Energy ϵ (eV)
$3\sigma_g^{-1}$
$1\pi_u^{-1}$
$1\pi_g^{-1}$
35
30
25
20
15
10
5
10
20
30
40
50
60
70

FIG.4

Appendix B

On π-Shell Photoionization in Molecular Nitrogen

T. N. Rescigno

Theoretical Atomic and Molecular Physics Group
University of California, Lawrence Livermore Laboratory
Livermore, California 94550

A. Gerwer and B. V. McKoy

A. A. Noyes Laboratory of Chemical Physics,
California Institute of Technology,
Pasadena, California 91125

and

P. W. Langhoff

Department of Chemistry
Indiana University
Bloomington, Indiana 47405

Abstract

Static-exchange calculations of π-shell photoionization in molecular nitrogen yield a physically incorrect description of the $1\pi_u \rightarrow k\pi_g$ partial-channel cross section; difficulties are attributed to spurious perturbations arising from the intense $\pi \rightarrow \pi^*$ intravalence transition. A simple projection procedure is devised that retains the computational simplicity of the frozen-core approximation and gives cross sections in good accord with measured values.

Introduction:

A recent series of articles reports static-exchange calculations of partial-channel photoionization cross sections in the diatomic molecules N_2, CO, O_2 and F_2 [1-6]. Although the results of these calculations are in generally good agreement with corresponding line-source [7-10], synchrotron radiation [11-13], and (e,2e) [14-16] measurements, discernable quantitative discrepancies between theory and experiment are evident in the cases of the $(1\pi_u^{-1})$ and $(1\pi^{-1})$ channels in N_2 and CO respectively. Because the separated-channel static-exchange approximation has proved to be otherwise satisfactory in studies of the outer-valence-shell photoelectron spectra [17] and photoionization cross sections of light diatomic [1-6] and polyatomic molecules [18-21], it is important to identify the origins of the discrepancy between theory and experiment in the $(1\pi_u^{-1})N_2$ and $(1\pi^{-1})CO$ channels.

In the present letter, the discrepancy between our previous results [2] and experiment in the case of the $1\pi_u$ channel in N_2 is investigated, and attributed to the presence of the strong $\pi\rightarrow\pi^*$ intravalence transition in the calculated spectrum. A simple procedure for avoiding the difficulties that can arise in this connection is suggested, and detailed applications are presented. In order to understand the origins of the difficulty, it is helpful to recall that strong mixing occurs between the $(\pi\pi^*)V_\pi$ and $(\sigma\sigma^*)V_\sigma$ configurational states in N_2 [22-24], resulting in low-lying and high-lying intravalence states in this case. The former corresponds to the $b'^1\Sigma_u^+$ state in N_2 with a vertical excitation energy of 14.4 eV [25], whereas the latter

corresponds to a strong photoionization resonance in the $(3\sigma_g \rightarrow k\sigma_u)$ $X^2\Sigma_g^+$ partial-channel cross section centered at $\simeq$ 28 eV [2]. Because the static-exchange model in N_2 does not include σ-π correlation or core relaxation, the $\pi \rightarrow \pi^*$ transition is uncorrectly located in the spectrum, producing a significant spurious perturbation of the corresponding Rydberg series and photoionization continuum. Moreover, the position of the V_π state is very sensitive to the specific form of the potential employed in the calculation, and it is shown here that the transition can be made to fall above or below the ionization threshold upon appropriate choice of potential. Consequently, caution must be exercised in applications of local exchange potential and related approximations to studies of molecular excitation/ionization spectra that include intravalence transitions.

To obtain a reliable approximation to the $1\pi_u \rightarrow k\pi_g$ photoionization cross section in N_2 in the presence of the strong N-V_π intravalence transition would require an extensive configuration-interaction study on states of $^1\Sigma_u^+$ symmetry in N_2, including the necessary σ-π interactions. In this letter, these important physical interactions are modelled by employing an approximate P-Q projection procedure within the framework of the static-exchange approximation. The procedure is similar to previous studies of autoionizing states in which a background continuous spectrum orthogonal to a zeroth-order compact localized state is constructed and employed in shift and width calculations [26]. When this approach is employed in N_2, using a $1\pi_g$ orbital obtained from a static-exchange $(1\pi_u^{-1}1\pi_g)\,^3\Sigma_u^+$ state calculation, the resulting $1\pi_u \rightarrow k\pi_g$ photoionization cross section is found to be relative-

ly insensitive to the potential employed and similar to the corresponding cross sections in O_2 and F_2 [4-6]. Moreover, the resulting partial-channel cross section for formation of $(1\pi_u^{-1})A^2\Pi$ parent N_2^+ ions is found to be in excellent agreement with the measured data [7,9,11,12,14,15] when a factor of two error in the previously reported $1\pi_u \rightarrow k\delta_g$ component [2] is also corrected.

The static-exchange calculations in N_2 are reported in section 2, comparisons are made with experiment in section 3, and some concluding remarks are made in section 4.

2. Static-exchange calculations in N_2:

In this section static-exchange calculations in N_2 are reported employing (i) a potential appropriate for closed-shell systems with non-degenerate orbitals, (ii) a properly equivalence-restricted potential appropriate for a closed $1\pi_u$ shell, and (iii) an equivalence-restricted potential with a background spectrum orthogonal to the $1\pi_g$ orbital.

The previously reported static-exchange calculations in N_2 involve solutions of the one-electron equation [1,2]

$$(T + V + V_{\pi_{ux}} - \epsilon)\phi_\epsilon = 0 \qquad (1)$$

Here, T and V are the kinetic-and nuclear-potential-energy operators, and

$$V_{\pi_{ux}} = \sum_i (2J_i - K_i) + J_{\pi_{ux}} + K_{\pi_{ux}} + 2J_{\pi_{uy}} - K_{\pi_{uy}} \qquad (2)$$

is the conventional static-exchange potential for excitation of a non-

degenerate orbital in a closed-shell system [27,28]. The sum over i includes all the doubly occupied canonical σ orbitals in N_2, but not the $1\pi_u$ shell in this case. The energy variable ε refers to discrete states below the ionization threshold, as well as photoionization states above the threshold.

In Fig. 1 curve (1) shows the partial-channel $1\pi_u \rightarrow n\pi_g/k\pi_g$ photoexcitation/ionization cross section in N_2 obtained from solution of eq. (1) employing a 27-term π_g basis set and the Stieltjec-Tchebycheff moment-theory technique [2,29]. The discrete spectrum is presented in the so-called Stieltjec sense [30], so that it joins on to the photoionization cross section at threshold, and the two can be treated on an equal footing. There is clearly a very strong $\pi \rightarrow \pi^*$ transition in the spectrum $\simeq$ 2.4eV below the ionization threshold of 16.7 eV [31]. In addition to this state, the compact valence portion of the basis set also contributes to the associated Rydberg series, the intensities of which are strongly perturbed, and to the corresponding photoionization cross section, the latter taking on a spuriously large value at threshold. What is needed to obtain a profile more in accord with reality is configuration mixing with the $(\sigma \rightarrow \sigma^*)$ states, which will reduce the spuriously large f number of the transition, but leave the position of the Rydberg series unchanged, thereby removing its perturbation and that of the continuum by the valence V_π state.

It is interesting to determine whether the spurious result for the $1\pi_u \rightarrow k\pi_g$ cross section can be attributed to an incorrect choice of potential in eq. (2). Indeed, the potential of eq. (2) is inappropri-

ate, since it involves only $1\pi_{ux} \rightarrow n\pi_{gx}/k\pi_{gx}$ excitation/ionization, and, consequently, does not take proper cognizance of the orbital-equivalence restriction [32]. An equivalence-restricted static-exchange potential is obtained from a wavefunction and energy functional involving both $\pi_{ux} \rightarrow \pi_{gx}$ and $\pi_{uy} \rightarrow \pi_{gy}$ symmetry components in the form [33]

$$V_{\pi_{ux}} = \sum_i (2J_i - K_i) + \tfrac{1}{2}J_{\pi_{ux}} + 3K_{\pi_{ux}} + 5/2J_{\pi_{uy}} - 5K_{\pi_{uy}}, \qquad (3)$$

where the sum over i includes all the σ orbitals in N_2. Of course, other symmetry restricted potentials can be devised that differ from that of eq. (3), although the latter gives results identical with those obtained from single-excitation configuration-interaction studies [34].

The $1\pi_u \rightarrow n\pi_g/k\pi_g$ photoexcitation/ionization cross section obtained from eqs. (1) and (3), employing the 27-term π_g basis set indicated above, is shown as curve (2) in fig. 1. There is a dramatic difference between this result and that of eqs. (1) and (2) in that the $\pi \rightarrow \pi^*$ transition now appears $\simeq$ 2eV above threshold in the photoionization continuum. It is highly unlikely that the use of a still larger basis set will significantly alter the photoionization cross section obtained from eqs. (1) and (3). Consequently, the position of the $\pi \rightarrow \pi^*$ transition in the spectrum is seen to be rather sensitive to the static-exchange potential [eqs. (2) or (3)], and an apparent "improvement" in the potential is seen to result in a highly unphysical cross section.

Since it is known that the $b'^1\Sigma_u^+$ state in N_2 falls below the $(1\pi_u^{-1})A^2\Pi_u$ ionization threshold, and it is clear that the transition significantly perturbs the static-exchange calculations, a projection procedure in which the $1\pi_g$ valence orbital is removed would seem to be appropriate. In this way the complexities of a configuration-interaction calculation can be avoided, the simplicity of the static-exchange approximation can be retained, and the usefulness of the projection procedure for describing the $1\pi_u \rightarrow k\pi_g$ photoionization cross section can be assessed.

A valence-like $1\pi_g$ orbital is obtained in the present development from calculations of the $(1\pi_u^{-1}1\pi_g)^3\Sigma_u^+$ state in the 27-term π_g basis indicated above. This orbital constitutes the P space, and the appropriate Q=1-P complement is obtained by direct orthogonalization of the basis to the $1\pi_g$ orbital, giving a 26-term π_g background basis set. Interest here is focused primarily on the photoionization continuum, which is expected to be less sensitive to the specific choice of $1\pi_g$ orbital than in corresponding $^1\Sigma_u^+(\pi \rightarrow \pi^*)$ state. Solutions of eq. (1) using both the eq. (2) and eq. (3) potentials are constructed in this orthogonalized basis. The two results are found to be virtually identical and are shown as curve (3) in fig. 1 The profile is seen to be quite weak compared to the two other results also shown in the figure, which latter contain significant contributions from the $1\pi_g$ valence orbital, as indicated above. By contrast, the $1\pi_u \rightarrow k\pi_g$ photoionization cross section obtained in the absence of the $1\pi_g$ valence orbital in N_2 is very similar to the corresponding results in O_2 and F_2 [4-6], in which cases the appropriate $1\pi_g$ valence orbitals

do not appear explicitly. Although the static-exchange results with projection are seen to be sensible, of course the ultimate test of the quantitative reliability of the calculated cross section is to be found in comparison with measurements.

3. Comparison with experiment:

The "projected" static-exchange calculations of the $1\pi_u \rightarrow k\pi_g$ cross section in N_2 described in the preceding section are combined with the previously reported $1\pi_u \rightarrow k\sigma_g$ and $k\delta_g$ components [2] and presented in fig. 2. It is seen that the $1\pi_u \rightarrow k\sigma_g$ contribution to the $1\pi_u^{-1}$ partial-channel cross section is relatively small, whereas the $1\pi_u \rightarrow k\delta_g$ component provides the dominant contribution. As indicated above, the $1\pi_u \rightarrow k\delta_g$ cross section of fig. 2 differs from that previously reported by a factor of two [2]. Evidently, the results so obtained are in very good agreement with the line-source [9], synchrotron-radiation [11,12], and (e,2e) [14] measurements also shown in the figure. By contrast, if either of the two $1\pi_u \rightarrow k\pi_g$ cross sections of fig. 1 [(1) and (2)] containing the $1\pi_g$ contribution are employed in fig. 2, the results so obtained for the $(1\pi_u^{-1})$ cross section are in significant disagreement with experiment.

In order to further clarify the range of validity if static-exchange calculations of photoionization cross sections in N_2, the partial-channel cross sections for production of $(3\sigma_g^{-1})X^2\Sigma_g^+$, $(1\pi_u^{-1})A^2\Pi_u$, and $(2\sigma_u^{-1})B^2\Sigma_u^+$ parent N_2^+ ions are compared with experiment in fig.3. The $(1\pi_u^{-1})A^2\Pi_u$ channel shown is taken from fig. 2, whereas the other two channels are taken from the previously reported studies [2]. It is seen that the three calculated results are in correspondingly

good agreement with the measured values. Moreover, the sum of the three results is also in good agreement with the independent (e, e + ion) measurements of the N_2^+ cross section [15].

4. Concluding remarks

In the present letter, discrepancies between theory and experiment in the $1\pi_u$ partial-channel photoionization cross section in N_2 reported previously are discussed and clarified [2]. These discrepancies are attributed, on the basis of the present study, to complications that can arise in static-exchange cross section calculations in the presence of strong intravalence transitions. It is shown that the static-exchange approximation to the $1\pi_u \rightarrow 1\pi_g$ transition in N_2 is rather sensitive to the particular noncentral, nonlocal potential employed, and that its presence in the calculated spectrum can strongly perturb the corresponding $1\pi_u \rightarrow k\pi_g$ photoionization cross section in an entirely spurious fashion. Because an incorrect multiplicity factor was employed for the $1\pi_u \rightarrow k\delta_g$ component in the $(1\pi_u^{-1})A^2\Pi_u$ partial-channel cross section, the previously reported results (ref. [2], figs. 2 and 6) do not appear to be in significant disagrement at threshold with the measured values.

A simple projection procedure is devised for calculation of the $1\pi_u \rightarrow k\pi_g$ photoionization cross section in N_2 in the presence of the strong $1\pi_u \rightarrow 1\pi_g$ intravalence transition. A valence-like $1\pi_g$ orbital obtained from static-exchange calculations of the $(1\pi_u^{-1}1\pi_g)^3\Sigma_u^+$ state is used in construction of a background π_g space for determination of the appropriate cross section. Although the $^1\Sigma_u^+(\pi \rightarrow \pi^*)$ state properties are expected to be highly sensitive to the choice of $1\pi_g$ orbital in this procedure, the corresponding background photoionization continuum should be less sensitive to orbital choice. The $1\pi_u \rightarrow k\pi_g$ cross section so obtained is found to be in-

sensitive to the specific static-exchange potential employed, is in excellent accord with measured values, and is consistent with the corresponding recently reported π-shell cross sections in O_2 and F_2 [4-6].

REFERENCES

[1] T. N. Rescigno and P. W. Langhoff, Chem. Phys. Letters 51 (1977) 65.

[2] T. N. Rescigno, C. F. Bender, B. V. McKoy and P. W. Langhoff, J. Chem. Phys. 68 (1978) 970.

[3] N. Padial, G. Csanak, B. V. McKoy and P. W. Langhoff, J. Chem. Phys. 69 (1978) 2992.

[4] A. Gerwer, C. Asaro, B. V. McKoy and P. W. Langhoff, J. Chem. Phys. (1979), to be published.

[5] P. W. Langhoff, A. Gerwer, C. Asaro and B. V. McKoy, Intern. J. Quantum Chem. S13 (1979), to be published.

[6] A. E. Orel, T. N. Rescigno, B. V. McKoy and P. W. Langhoff, J. Chem. Phys. (1979), to be published.

[7] R. L. Blake and J. H. Carver, J. Chem. Phys. 47 (1967) 1038.

[8] J. A. R. Samson and J. L. Gardner, J. Electron Spectry. 8 (1976) 35.

[9] J. A. R. Samson, G. N. Haddad and J. L. Gardner, J. Phys. B 10 (1977) 1749.

[10] J. A. R. Samson, J. L. Gardner and G. N. Haddad, J. Electron Spectry. 12 (1977) 281.

[11] P. R. Woodruff and G. V. Marr, Proc. Roy. Soc. A 358 (1977) 87.

[12] E. W. Plummer, T. Gustafsson, W. Gudat and D. E. Eastman, Phys. Rev. A 15 (1977) 2339.

[13] T. Gustafsson, private communication.

[14] A. Hamnett, W. Stoll and C. E. Brion, J. Electron Spectry. 8 (1976) 367.

[15] G. R. Wright, M. J. van der Wiel and C. E. Brion, J. Phys. B 9 (1976) 675.

[16] C. E. Brion, K. H. Tan, M. J. van der Wiel and Ph. E. van der Leeuw, J. Electron Spectry. (1979), to be published.

[17] L. S. Cederbaum and W. Domcke, Advan. Chem. Phys. 36 (1978) 205.

[18] P. W. Langhoff, A. E. Orel, T. N. Rescigno and B. V. McKoy, J. Chem. Phys. 69 (1978) 4689.

[19] G. R. J. Williams and P. W. Langhoff, Chem. Phys. Letters 60 (1978) 201.

[20] N. Padial, G. Csanak, B. V. McKoy and P. W. Langhoff, J. Chem. Phys., to be published.

[21] N. Padial, G. Csanak, B. V. McKoy and P. W. Langhoff, J. Chem. Phys., to be published.

[22] R. S. Mulliken, Chem. Phys. Letters 25 (1974) 305; 46 (1977) 197.

[23] R. S. Mulliken, Accounts Chem. Res. 9 (1976) 7.

[24] R. S. Mulliken and W. C. Ermler, Diatomic molecules (Academic Press, New York 1977).

[25] J. Geiger and B. Schroder, J. Chem. Phys. 50 (1969) 7.

[26] U. Fano, Phys. Rev. 124 (1961) 1866.

[27] P. W. Langhoff, M. Karplus and R. P. Hurst, J. Chem. Phys. 44 (1966) 505.

[28] W. J. Hunt and W. A. Goddard, Chem. Phys. Letters 3 (1969) 414.

[29] P. W. Langhoff, in: Electron-molecule and photon-molecule collisions, ed. T. Rescigno, V. McKoy and B. Schneider (Plenum Press, New York, 1979) pp.183-224.

[30] P. W. Langhoff and C. T. Corcoran, J. Chem. Phys. 61 (1974) 146.

[31] D. W. Turner, C. Baker, A. D. Baker and C. R. Brundle, Molecular photoelectron spectroscopy (Wiley, New York, 1970).

[32] C. C. J. Roothaan, Rev. Mod. Phys. 32 (1960) 179.

[33] J. B. Rose and V. McKoy, J. Chem. Phys. 55 (1971) 5435.

[34] H. Lefebrve-Brion, C. Moser and R. K. Nesbet, J. Mol. Spectry. 13 (1964) 418.

FIGURE CAPTIONS

Fig. 1. Static-exchange calculations of $1\pi_u \rightarrow n\pi_g/k\pi_g$ photoexcitation/ionization cross section in N_2: (1) values obtained using eqs. (1) and (2) without $1\pi_g$ projection; (2) values obtained using eqs. (1) and (3) without $1\pi_g$ projection; (3) values obtained using eqs. (1) and (2) or (3) with $1\pi_g$ projection, as discussed in the text. 1 Mb = 10^{-18} cm^2.

Fig. 2. Partial-channel $1\pi_u \rightarrow k\sigma_g$, $k\pi_u$, $k\delta_u$ components and $(1\pi_u^{-1})A^2\Pi_u$ photoionization cross section in N_2: (—) static-exchange calculation, including $1\pi_g$ projection in the $k\pi_g$ component and correcting a factor of two error in the $k\delta_g$ component [2]; (●) line source measurements [9]; (▲) (e, 2e) measurements [14]; (■) synchrotron radiation measurements [11, 12].

Fig. 3. Total and partial-channel photoionization cross sections in N_2 for production of $(3\sigma_g^{-1})X^2\Sigma_g^+$, $(1\pi_u^{-1})A^2\Pi_u$, and $(2\sigma_u^{-1})B^2\Sigma_u^+$ parent N_2^+ ions: (—) static-exchange calculations, including $1\pi_g$ projection in the $k\pi_g$ channel; (▲,■) as in fig. 2; (●) total cross section for N_2^+ photoproduction [15].

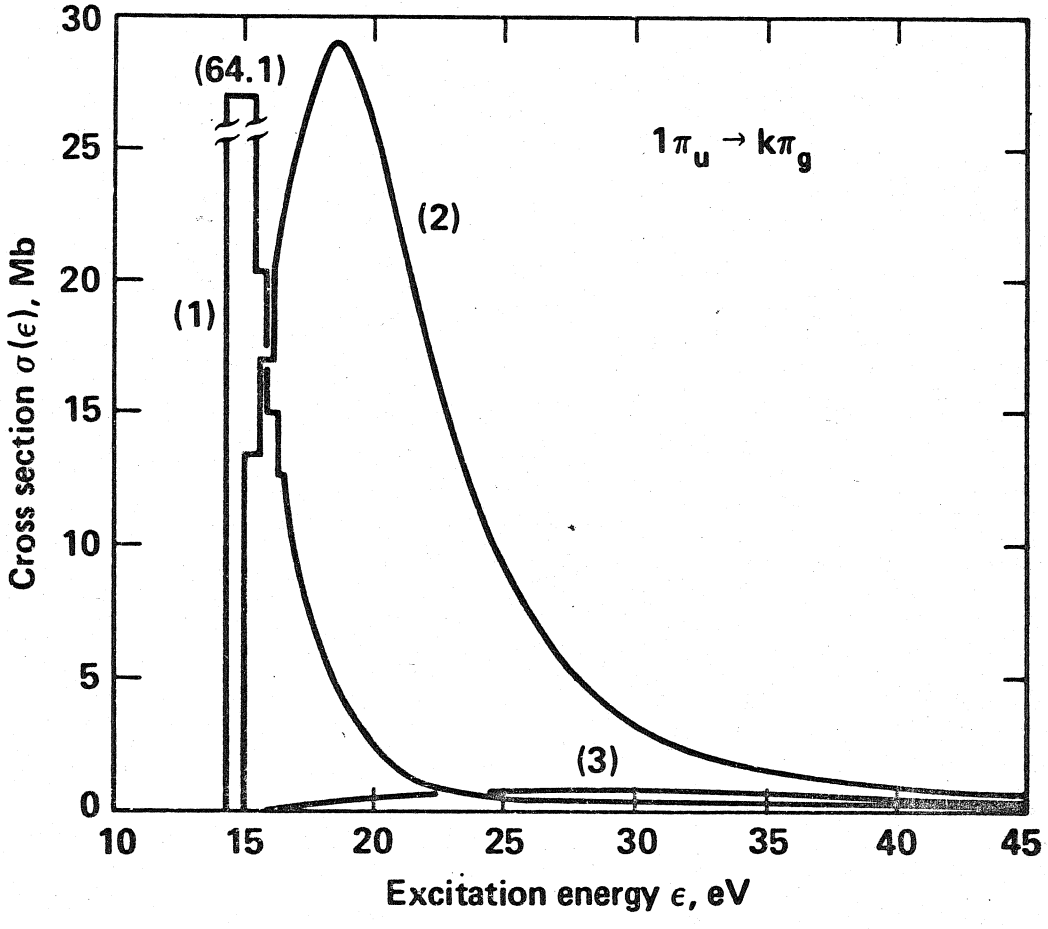
30
25
20
15
10
5
0
(64.1)
(1)
(2)
(3)
$1\pi_u \rightarrow k\pi_g$
Cross section $\sigma(\epsilon)$, Mb
10
15
20
25
30
35
40
45
Excitation energy ϵ, eV

FIG.1

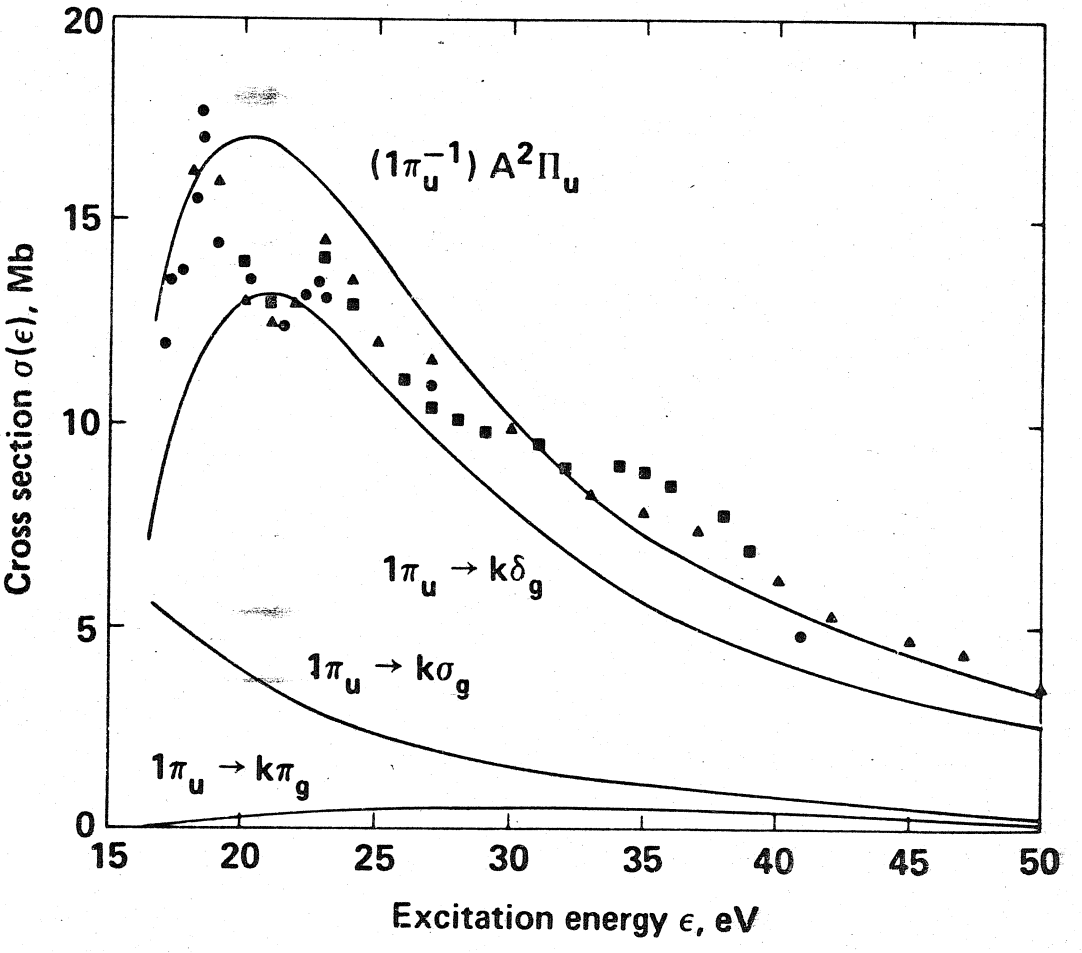
20
15
10
5
0
15
20
25
30
35
40
45
50
Cross section σ(ϵ), Mb
Excitation energy ϵ, eV
$(1\pi_u^{-1})\ A^2\Pi_u$
$1\pi_u \rightarrow k\delta_g$
$1\pi_u \rightarrow k\sigma_g$
$1\pi_u \rightarrow k\pi_g$

FIG.2

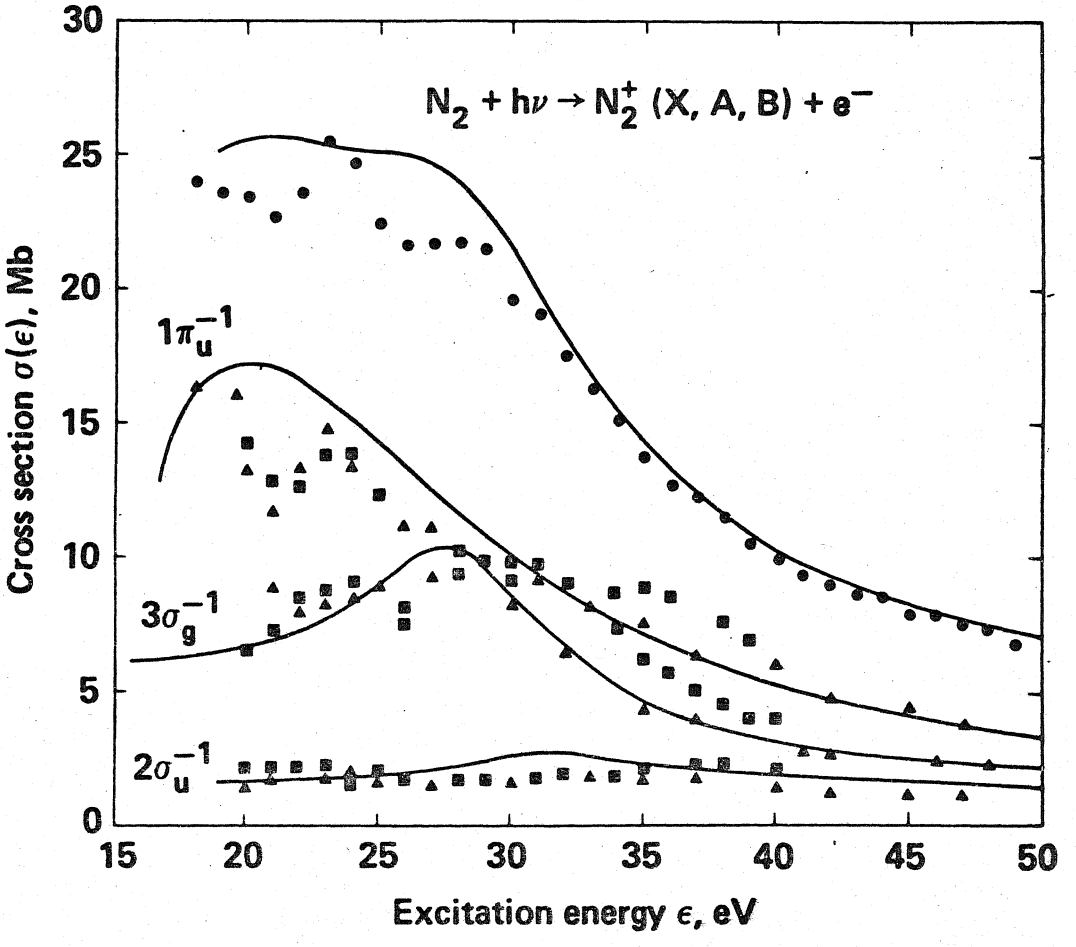
$N_2 + h\nu \rightarrow N_2^+ (X, A, B) + e^-$
$1\pi_u^{-1}$
$3\sigma_g^{-1}$
$2\sigma_u^{-1}$
Cross section $\sigma(\epsilon)$, Mb
Excitation energy ϵ, eV
0
5
10
15
20
25
30
15
20
25
30
35
40
45
50

FIG.3